

# Post-translational control of T cell development by the ESCRT protein CHMP5

Stanley Adoro<sup>1,2</sup>, Kwang Hwan Park<sup>3,9</sup>, Sarah E Bettigole<sup>4</sup>, Raphael Lis<sup>5</sup>, Hee Rae Shin<sup>4</sup>, Heewon Seo<sup>6</sup>✉, Ju Han Kim<sup>6</sup>, Klaus-Peter Knobeloch<sup>7</sup>, Jae-Hyuck Shim<sup>8</sup> & Laurie H Glimcher<sup>1,2</sup>

The acquisition of a protective vertebrate immune system hinges on the efficient generation of a diverse but self-tolerant repertoire of T cells by the thymus through mechanisms that remain incompletely resolved. Here we identified the endosomal-sorting-complex-required-for-transport (ESCRT) protein CHMP5, known to be required for the formation of multivesicular bodies, as a key sensor of thresholds for signaling via the T cell antigen receptor (TCR) that was essential for T cell development. CHMP5 enabled positive selection by promoting post-selection thymocyte survival in part through stabilization of the pro-survival protein Bcl-2. Accordingly, loss of CHMP5 in thymocyte precursor cells abolished T cell development, a phenotype that was ‘rescued’ by genetic deletion of the pro-apoptotic protein Bim or transgenic expression of Bcl-2. Mechanistically, positive selection resulted in the stabilization of CHMP5 by inducing its interaction with the deubiquitinase USP8. Our results thus identify CHMP5 as an essential component of the post-translational machinery required for T cell development.

T cells arise in the thymus from precursor CD4<sup>+</sup>CD8<sup>+</sup> double-positive (DP) thymocytes through the process of positive selection, which is initiated by low-affinity interactions between their surface TCR and intrathymic major histocompatibility complex (MHC) molecules loaded with self peptide. High-affinity interactions, in contrast, cause ‘negative selection’ by inducing apoptosis of DP thymocytes that have received such signaling<sup>1</sup>. Regardless of the MHC specificity of the DP thymocyte that has received signaling, a chief consequence of positive selection is that it induces an anti-apoptotic program, including expression of the pro-survival protein Bcl-2, that enables selected thymocytes to survive and complete their maturation<sup>1,2</sup>. Despite growing evidence of the key molecules that control thymocyte selection signaling and the transcription factors that establish the various T cell lineages, the cellular machinery that integrates and sustains the pro-survival program in post-selection thymocytes is not fully understood.

Proteasome-dependent post-translational regulatory mechanisms that control the turnover of complexes of the TCR and its invariant chain CD3 and apoptosis have long been recognized as critical regulators of thymocyte development<sup>3,4</sup>. However, even though inhibition of proteasome activity stabilizes pro-survival proteins to prevent the apoptosis induced by TCR agonists or glucocorticoids that leads to thymocyte differentiation<sup>4,5</sup>, it can also stabilize pro-apoptotic proteins and death-associated caspases to impair thymocyte maturation<sup>6</sup>. Such observations highlight the complexity of the cellular post-translational

machinery and suggest that the post-translational regulation in thymocytes must be very finely tuned in response to appropriate TCR selection signals to achieve the desired developmental fates.

Originally identified in yeast, the ESCRT machinery comprises a large family of proteins that together orchestrate the membrane-deformation and membrane-scission events required for the formation of multivesicular bodies (MVBs), endocytosis and retroviral budding in eukaryotic cells<sup>7</sup>. In the most basic setting, ESCRT complexes are recruited sequentially (from ESCRT-0 to ESCRT-III) onto the surface of endosomal membranes with ubiquitinated transmembrane cargoes, which leads to their being sorted into membrane-delimited intraluminal vesicles within MVBs<sup>7</sup>. The rate-limiting critical final step, which involves disassembly of the ESCRT complex and scission of the nascent delimited membrane vesicle, is mediated by the AAA-ATPase complex VPS4 in a reaction that requires accessory ESCRT proteins, including CHMP5 (also known as VPS60 or MOS10)<sup>8,9</sup>. Yeast *vps60*-null mutants have disrupted endocytic sorting<sup>10</sup>, and CHMP5-deficient mouse embryonic cells have enlarged late endosomes that fail to form lysosomes, which results in impaired receptor downregulation<sup>11</sup>, consistent with a role for CHMP5 in the ESCRT machinery. However, CHMP5 suppresses ubiquitination of the inhibitor IκBα in osteoclasts without any alteration in the endocytic pathway<sup>12</sup>, which indicates that the function of individual ESCRT proteins probably extends beyond their membrane-remodeling activity.

<sup>1</sup>Department of Cancer Immunology and Virology, Dana Farber Cancer Institute, Boston, Massachusetts, USA. <sup>2</sup>Department of Medicine, Harvard Medical School, Boston, Massachusetts, USA. <sup>3</sup>Department of Pathology, Weill Cornell Medicine, New York, New York, USA. <sup>4</sup>Quentis Therapeutics, New York, New York, USA. <sup>5</sup>Ansary Stem Cell Institute, Department of Genetic Medicine, Weill Cornell Medicine, New York, New York, USA. <sup>6</sup>Division of Biomedical Informatics, Seoul National University College of Medicine, Seoul, South Korea. <sup>7</sup>Institute for Neuropathology, University of Freiburg, Freiburg, Germany. <sup>8</sup>Division of Rheumatology, Department of Medicine, University of Massachusetts Medical School, Worcester, Massachusetts, USA. <sup>9</sup>Present address: Department of Orthopedic Surgery, Yonsei University College of Medicine, Seoul, South Korea. Correspondence should be addressed to L.H.G. (laurie\_glimcher@dfci.harvard.edu) or J.H.S. (jaehyuck.shim@umassmed.edu).

Received 18 April; accepted 3 May; published online 29 May 2017; doi:10.1038/ni.3764

Here we identified CHMP5 as an essential component of the positive-selection machinery required for T cell development. Beyond its role in MVB formation, we discovered a non-canonical post-translational activity of CHMP5 that prevented oxidation and degradation of Bcl-2 to ensure the post-selection survival of thymocytes. That CHMP5 activity ‘mapped’ specifically to the intermediate-thymocyte stage of development. As lack of CHMP5 in thymocyte precursor cells completely abolished T cell maturation, our findings reveal an unexpected and previously unknown thymocyte developmental checkpoint in which post-translational stabilization of CHMP5 enables the completion of positive selection.

## RESULTS

### CHMP5 expression in developing thymocytes

While assessing ubiquitin-regulated proteins in thymocytes, we discovered that CHMP5 was stabilized by the proteasome inhibitor MG132 in a manner that paralleled MG132-dependent stabilization of proteins of the Bcl-2 family<sup>13,14</sup> (**Supplementary Fig. 1a,b**), suggestive of a potential role for CHMP5 in T cell development. Analysis of the expression of *Chmp5* mRNA and CHMP5 protein in sorted thymocytes revealed that CHMP5 was post-transcriptionally regulated, with the highest protein expression in intermediate (CD4<sup>+</sup>CD8<sup>lo</sup>CD24<sup>hi</sup>TCR $\beta^{int-hi}$ CD69<sup>+</sup>) thymocytes (**Fig. 1a,b**), which represent the post-selection ‘lineage-decision’ checkpoint and are the immediate precursors of mature T cells<sup>2</sup>. TCR-induced selection might uniquely modulate CHMP5, as the expression of representative proteins of the ESCRT family changed only modestly in developing thymocytes (**Supplementary Fig. 1c**). Thymocyte expression of CHMP5 protein and *Chmp5* mRNA was independent of TCR specificity, as it was induced in thymocytes that received MHC class I signaling and those that received MHC class II signaling in mice deficient in the MHC class II molecule H-2A<sup>b</sup> (*H2-Ab1*<sup>-/-</sup>) and mice deficient in the MHC class I molecule  $\beta_2$ -microglobulin (*B2m*<sup>-/-</sup>), respectively (**Fig. 1c** and **Supplementary Fig. 1d**). Thus, the induction of CHMP5 protein was associated with the positive selection of thymocytes.

### T cell development requires CHMP5

To determine the function of CHMP5 during T cell development, we crossed mice with *loxP*-flanked alleles encoding CHMP5 (*Chmp5*<sup>f/f</sup>)<sup>12</sup> to mice with transgenic expression of Cre recombinase from the promoter of the T cell-specific gene *Cd4* (*Cd4-Cre*) to generate mice with conditional deletion of CHMP5 in thymocytes (called ‘conditional knockout’ (CKO) mice here) (**Fig. 2a** and **Supplementary Fig. 1e**). The CKO mice were born at normal Mendelian ratios and showed no gross abnormalities relative to the phenotype of their *Chmp5*<sup>f/f</sup> littermates (called ‘wild-type’ here) or that of *Chmp5*<sup>f/f</sup>/*Cd4-Cre* mice, which were phenotypically identical to the wild-type mice (data not shown). Of note, loss of CHMP5 did not alter expression of genes encoding other ESCRT proteins (**Supplementary Fig. 1f**). However, histological analysis of CKO mice revealed a thymus with a considerably disorganized architecture and fragmented medullary regions (**Fig. 2b**), suggestive of defects in positive selection<sup>15</sup>. Despite having a normal number of DP thymocytes, CKO mice showed a striking loss of mature (CD24<sup>lo</sup>TCR $\beta^{hi}$ ) thymocytes, including CD4<sup>+</sup> or CD8<sup>+</sup> single-positive cells (**Fig. 2c** and **Supplementary Fig. 2a**). Similarly, the peripheral lymphoid organs, such as the lymph nodes and spleen, of the CKO mice were almost completely devoid of  $\alpha\beta$  T cells (**Fig. 2d,e**). The few residual T cells in these mice had failed to delete CHMP5 and were CD44<sup>hi</sup> (**Supplementary Fig. 2b,c**), reflective of T cell lymphopenia in these mice.

The pre- and post-positive-selection stages of thymocyte development are marked by upregulation of surface expression of the activation

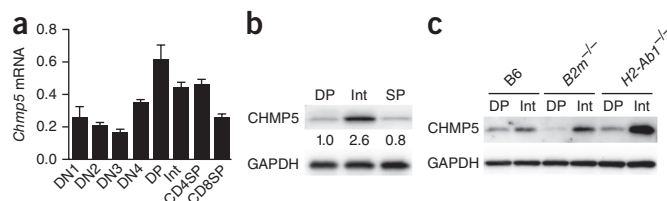


**Figure 1** CHMP5 expression in thymocytes. (a) *Chmp5* mRNA in subsets (horizontal axis) of thymocytes at CD4<sup>-</sup>CD8<sup>-</sup> double negative (DN) stages 1–4 (DN1–DN4), CD4<sup>+</sup>CD8<sup>+</sup> double-positive thymocytes (DP), intermediate thymocytes (Int), and CD4<sup>+</sup> (CD4SP) or CD8<sup>+</sup> (CD8SP) single-positive thymocytes; results are normalized to those of the control gene *Actb*. (b) Immunoblot analysis of CHMP5 and GAPDH (loading control throughout) in lysates of thymocytes of various subsets (above lanes); numbers below lanes indicate band intensity relative to that of DP thymocytes. (c) Immunoblot analysis of CHMP5 in C57BL/6 (B6), *B2m*<sup>-/-</sup>, and *H2-Ab1*<sup>-/-</sup> thymocytes (above blot) of various subsets (above lanes). Data are representative of three (a,b) or two (c) independent experiments (error bars (a), s.d. of biological duplicates).

marker CD69 and the TCR on thymocytes<sup>16,17</sup>. Quantification of thymocyte subsets by those markers revealed a normal number of pre-selection (CD69<sup>-</sup>TCR $\beta^{neg-lo}$ ) thymocytes but considerably fewer intermediate (CD69<sup>+</sup>TCR $\beta^{hi}$ ) thymocytes and post-selection (CD69<sup>-</sup>TCR $\beta^{hi}$ ) thymocytes in CKO mice relative to the abundance of these cells in wild-type mice (**Fig. 2f,g**). This analysis thus ‘mapped’ the earliest defect and requirement for CHMP5 to the intermediate post-selection thymocyte stage.

To further clarify the role of CHMP5 in the positive selection of thymocytes, we bred the CKO mice to OT-II mice (which have transgenic expression of an MHC class II (I-A<sup>b</sup>)-restricted TCR), in which clonotypic V $\alpha$ 2<sup>+</sup>V $\beta$ 5<sup>+</sup> T cells are positively selected into the CD4<sup>+</sup> T cell lineage<sup>18</sup>. Indeed, consistent with an essential requirement for CHMP5 in positive selection, the thymus and periphery of OT-II CKO mice showed considerable depletion of mature clonotypic V $\beta$ 5<sup>+</sup> thymocytes and V $\beta$ 5<sup>+</sup> T cells (**Fig. 2h** and **Supplementary Fig. 2d,e**). Collectively, these results revealed CHMP5 to be a cellular factor that was critically required for the positive selection of thymocytes and successful T cell development.

### Cell-intrinsic role for CHMP5 in positive selection

The ESCRT machinery can mediate non-cell-autonomous signaling<sup>19</sup>, which prompted us to assess whether the function of CHMP5 was cell intrinsic. For this, we generated mixed-bone-marrow chimeras by reconstituting lethally irradiated congenic (CD45.1<sup>+</sup>) host mice with a 1:1 ratio of bone marrow from wild-type (CD45.2<sup>+</sup>) or CKO (CD45.2<sup>+</sup>) donors and congenic B6.SJL (CD45.1<sup>+</sup>) donors (**Supplementary Fig. 3a**). Flow cytometry of cells from the thymus and spleen revealed that although B6.SJL and CKO donor cells generated a similar proportion of DP thymocytes, mature thymocyte and peripheral T cell populations were composed almost entirely of wild-type (CD45.1<sup>+</sup>) cells in chimeras reconstituted with a mixture of CKO and wild-type donor bone marrow (**Fig. 3a,b**).

To further confirm the cell-intrinsic activity of CHMP5 that was suggested by the preceding experiments, we assessed the restoration of thymocyte development in CKO mice by CHMP5 transgenesis. We constructed chimeras by reconstituting lethally irradiated B6.SJL (CD45.1<sup>+</sup>) mice with bone marrow cells transduced with bicistronic lentiviral vectors expressing green fluorescent protein (GFP) alone (control vector) or GFP and CHMP5 (**Supplementary Fig. 3b**). Analysis of CD45.2<sup>+</sup>GFP<sup>+</sup> CKO donor cells in fully reconstituted host mice revealed that transgenically expressed CHMP5 restored

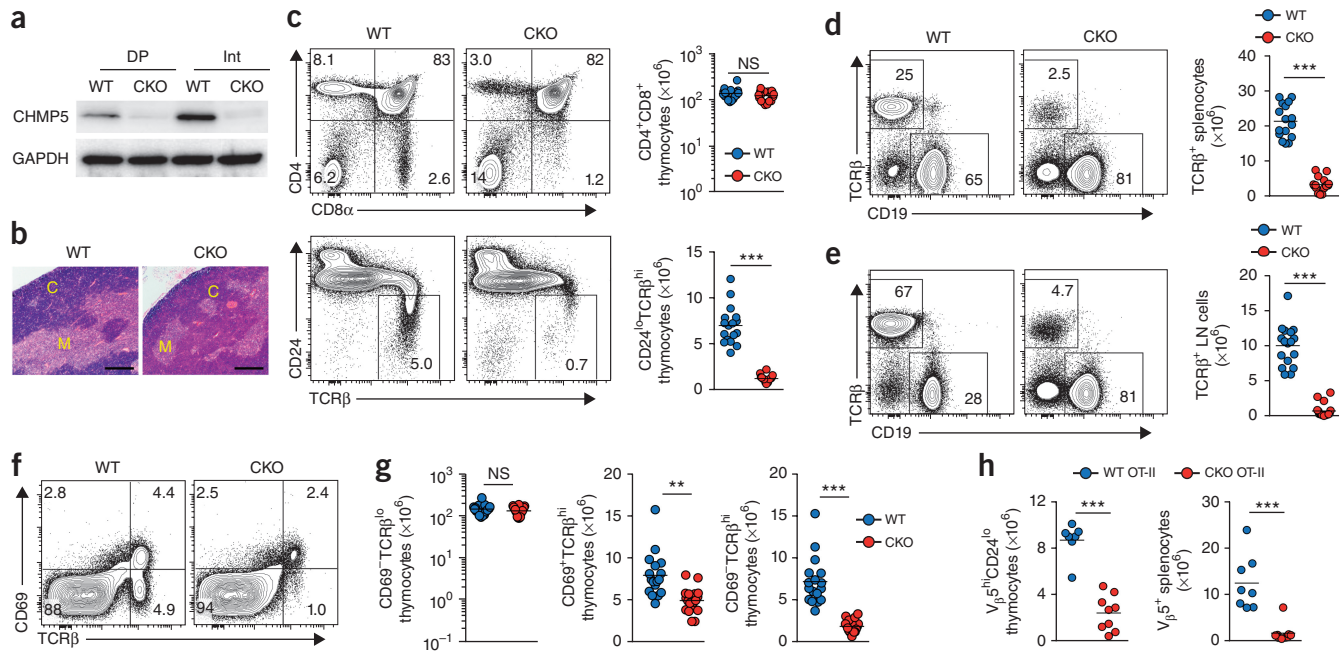


**Figure 2** CHMP5 is required for T cell development. **(a)** Immunoblot analysis of CHMP5 in sorted thymocyte subsets (above blots) from wild-type and CKO mice (above lanes). **(b)** Histology of wild-type and CKO thymus. M, medulla; C, cortex. Scale bars, 200  $\mu$ m. **(c–e)** Flow cytometry (left) analyzing the expression of CD4 versus CD8 $\alpha$  (top) or the cell-surface marker CD24 versus TCR $\beta$  (bottom) by wild-type and CKO thymocytes (**c**), and or of TCR $\beta$  versus the signal-transduction receptor CD19 by splenocytes (**d**) and lymph node (LN) cells (**e**) from wild-type and CKO mice, and absolute number of cells (right), gated as at left, from wild-type mice ( $n = 17$ ) and CKO mice ( $n = 18$ ). Numbers in quadrants (**c**, top) indicate percent cells in each throughout; numbers in outlined areas indicate percent CD24 $^{lo}$ TCR $\beta^{hi}$  (mature) thymocytes (**c**, bottom), or TCR $\beta^{+}$ CD19 $^{-}$  (top left) or TCR $\beta^{+}$ CD19 $^{+}$  (bottom right) cells (**d,e**). NS, not significant ( $P > 0.05$ ; 0.2186 in **c**); \*\*\* $P < 0.0001$  (Student's *t*-test). **(f,g)** Flow cytometry analyzing the expression of CD69 versus TCR $\beta$  by total thymocytes from wild-type and CKO mice (**f**), and absolute number of thymocyte subsets gated as in **(g)**. NS,  $P = 0.2737$ ; \*\* $P < 0.001$  (0.0002 in **g**) and \*\*\* $P < 0.0001$  (Student's *t*-test). **(h)** Quantification of clonotypic V $\beta$ 5 $^{+}$  mature (CD24 $^{lo}$ ) thymocytes (left) and splenic T cells (right) in OT-II wild-type mice ( $n = 7$ ) and OT-II CKO mice ( $n = 8$ ). \*\*\* $P < 0.0001$  (Student's *t*-test). Each symbol (**c–e,g,h**) represents an individual mouse; small horizontal lines indicate the mean. Data are representative of three independent experiments (**a,b**) or are pooled from four (**c–g**) or three (**h**) experiments.

the generation of T cells from CKO thymocytes (Fig. 3c,d and Supplementary Fig. 3c,d); these results established a cell-intrinsic function for CHMP5 in thymocytes.

#### Normal TCR signaling in CHMP5-deficient thymocytes

CKO thymocytes had surface expression of TCR $\beta$  and CD3 $\epsilon$  comparable to that of wild-type thymocytes (Fig. 4a,b). After crosslinking with antibody to TCR (anti-TCR) plus anti-CD4, purified CKO pre-selection DP thymocytes showed no defect in the phosphorylation of proximal TCR-signaling substrates, including LAT, ZAP-70 and Cbl (Fig. 4c). The upregulation of CD69 expression after antibody crosslinking was also similar wild-type pre-selection DP thymocytes and their CKO counterparts (Fig. 4d and Supplementary Fig. 4). Concordantly, *ex vivo* thymocyte analysis revealed similar expression of the TCR-signaling-avidity marker CD5 (ref. 20) (Fig. 4e,f) and markers of positive selection, the chemokine receptor CCR7 and cytokine receptor subunit IL-7R $\alpha$ <sup>16,21,22</sup> (Supplementary Fig. 4), on wild-type and CKO thymocytes.

While the results above indicated normal TCR signaling in CKO thymocytes, we nonetheless considered that differences in TCR signaling can be masked under polyclonal agonist stimulation<sup>23</sup>. Thus, we further assessed signaling in the well-characterized OT-I model deficient in MHC class I (OT-I B2m $^{-/-}$ ), in which preselection DP thymocytes can be activated with tetramer ligands of H-2K $\beta$  and ovalbumin (OVA) peptide with defined TCR affinities<sup>23,24</sup>. The kinetics of phosphorylation of the kinase ERK, a determinant of positive versus negative TCR selection<sup>25</sup>, were similar in wild-type thymocytes and CKO

thymocytes in response to a high-affinity tetramer (H-2K $\beta$ -OVA; agonist) or low-affinity tetramer (H-2K $\beta$ -Q7; antagonist) (Fig. 4g). Given the normal surface TCR density and surface expression of the TCR-signaling indicator CD5 (ref. 20) in CKO thymocytes (Fig. 4e,f), these data suggested that CHMP5 was dispensable for TCR signaling and that it enabled positive selection events distal to ERK.

Genome-wide analysis by RNA-based next-generation sequencing yielded few differences between the transcriptome of wild-type thymocytes and that of CKO thymocytes (data not shown), which indicated that CHMP5 might regulate T-cell development post-transcriptionally. We detected changes in transcript expression consistent with normal positive selection TCR signaling<sup>26</sup>, including the induction of *Gata3*, *Nfatc1*, *Egr1* and *Tox* (Supplementary Fig. 5a,b). Notably, while their differentiation was eventually abolished, CKO intermediate thymocytes initiated the transcription of genes (*Zbtb7b* and *Runx3*) encoding products linked to commitment to the CD4 $^{+}$  and CD8 $^{+}$  T cell lineages<sup>27</sup>, but with lower expression than that of mature lineage-committed thymocytes (Supplementary Fig. 5c). Thus, in intermediate thymocytes, CHMP5 acted at a point preceding terminal lineage commitment. Furthermore, unlike osteoclasts<sup>12</sup>, CKO thymocytes showed normal activity of the transcription actor NF- $\kappa$ B (Supplementary Fig. 5d,e) that is important for thymocyte development<sup>28,29</sup>.

#### ESCRT-dependent trafficking in thymocytes

The ESCRT machinery mediates the trafficking and endocytosis of surface receptors<sup>30</sup>. Despite its role in regulating the ATPase VPS4

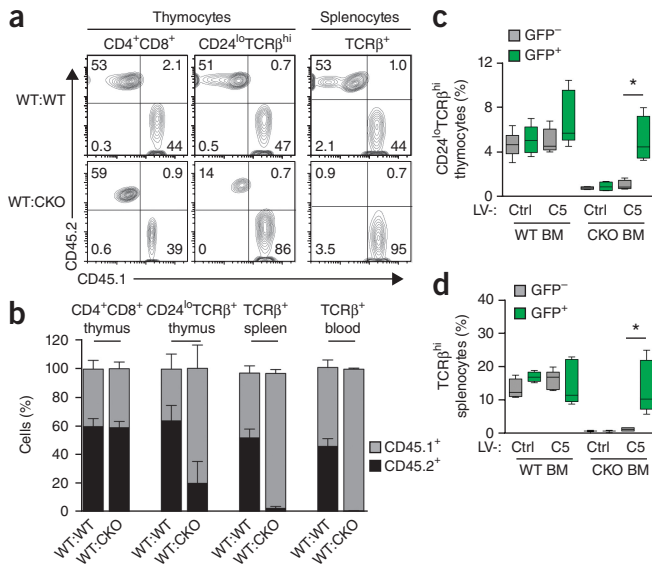


**Figure 3** Cell-intrinsic requirement for CHMP5 in positive selection. **(a)** Flow cytometry analyzing expression of the congenic markers CD45.2 and CD45.1 by thymocytes and splenocytes (above plots) from host chimeras reconstituted with a mixture of wild-type (CD45.2+) and wild-type (CD45.1+) donor bone marrow (WT:WT) or CKO (CD45.2+) and wild-type (CD45.1+) donor bone marrow (WT:CKO) (left margin). **(b)** Frequency of CD45.1+ or CD45.2+ cells (key) among various cell subsets (above plots) from the thymus, spleen and blood of chimeras as in **a** (horizontal axis). **(c,d)** Frequency of donor-derived mature GFP+ (transduced) or GFP- (non-transduced) (key) CD24 $^{lo}$ TCR $\beta^+$  thymocytes (**c**) or TCR $\beta^+$  splenocytes (**d**) from host chimeras reconstituted with wild-type or CKO donor (CD45.2+) bone marrow (BM) (below plots) transduced with control bicistronic lentivirus (LV-Ctrl) or bicistronic lentiviral vector expressing CHMP5 (LV-C5) (horizontal axis). \*P < 0.01 (0.0089 (**c**) or 0.0033 (**d**)) (Student's *t*-test). Data are representative of three independent experiments (average + s.e.m. of n = 5 mice per group in **b**; mean (center line), minimum and maximum (box ends), and highest and lowest values (bars extending above and below box) of n = 4–6 mice per group in **c,d**).

that catalyzes the final step in membrane scission during ESCRT activity<sup>31,32</sup>, we found that CHMP5 was unexpectedly dispensable for TCR dynamics in thymocytes. First, downregulation of surface clonotypic V $\alpha$ 2 $^+$  TCR on pre-selection thymocytes stimulated with tetramers of varying affinity proceeded normally (Fig. 5a). In addition, steady-state recycling of CD3e and internalization of CD3e complexes into early (EEA-1 $^+$ ) and late (Rab-7 $^+$ ) endosomal vesicles after TCR stimulation was unperturbed in CKO thymocytes (Fig. 5b,c). Furthermore, we assessed canonical ESCRT-mediated formation of MVBs and found that wild-type intermediate thymocytes and CKO intermediate thymocytes contained a similar number of MVBs of comparable size and a similar composition of intraluminal vesicles (Fig. 5d–g). These results together suggested that CHMP5 was dispensable for ESCRT activity in thymocytes.

#### CHMP5 promotes the survival of post-selection thymocytes

Failure in positive selection generally ‘maps’ to defects in either TCR signaling or thymocyte survival<sup>1,23,33,34</sup>. Because CHMP5 deficiency did not affect TCR signaling, we investigated whether it affected thymocyte survival. Notably, we found that CKO mice had a significantly higher frequency of apoptotic annexin V-positive post-selection thymocytes than wild-type mice had (Fig. 6a). To understand the basis of the enhanced apoptosis of CKO thymocytes, we evaluated the expression

of proteins of the Bcl-2 family that are essential for the survival and development of thymocytes<sup>35</sup>. Although CKO thymocytes exhibited expression of mRNA encoding pro-survival proteins of the Bcl-2 family (Fig. 6b and Supplementary Fig. 6a) and mRNA encoding the pro-apoptotic protein Bim (Supplementary Fig. 6a,b) similar to that of wild-type thymocytes, we found that total and mitochondrial Bcl-2 proteins were much less abundant in polyclonal thymocytes and in clonotypic OT-II CKO thymocytes than in their wild-type counterparts (Fig. 6c and Supplementary Fig. 6b–e).

IL-7, a key inducer of Bcl-2 expression in intermediate thymocytes<sup>2</sup>, induced normal phosphorylation of the transcription factor STAT5 but failed to restore the expression of Bcl-2 protein in CKO thymocytes (Supplementary Fig. 6f,g), which indicated that the defective expression of Bcl-2 protein was not due to a failure of signaling via the IL-7 receptor. In cultures treated with cycloheximide to block all new protein synthesis, we found that CKO thymocytes had more degradation of Bcl-2 protein than that of wild-type thymocytes (Supplementary Fig. 6h). Together these biochemical results were consistent with a post-translational defect in Bcl-2 expression in CHMP5-deficient thymocytes.

#### Post-translational regulation of Bcl-2 stability by CHMP5

We next sought to elucidate the Bcl-2–CHMP5 interaction and its mechanism of action. Co-immunoprecipitation of proteins with anti-CHMP5 revealed that endogenous CHMP5 associated with Bcl-2 in intermediate thymocytes (Fig. 6d). The physical interaction of Bcl-2 and CHMP5 was further confirmed in HEK293 human embryonic kidney cells co-expressing epitope-tagged Bcl-2 and CHMP5 (Supplementary Fig. 6i). This interaction probably involved direct contact, as we detected Bcl-2–CHMP5 interactions in a cell-free assay (Supplementary Fig. 6j).

Since post-translational inactivation and degradation of Bcl-2 involves reactive oxygen species (ROS)-mediated oxidation of its cysteine residues into cysteine sulfenic acid<sup>36</sup>, we assessed such sulfenylation of Bcl-2 in thymocytes. For this, we immunoprecipitated Bcl-2 from total thymocyte lysates with anti-Bcl-2 (normalized by equal amounts of Bcl-2 in the input samples) and quantified sulfenylation in the immunoprecipitates with the biotinylated sulfenic-acid-reactive probe DCP-Bio1, followed by streptavidin-based detection<sup>37</sup>. Notably, Bcl-2 immunoprecipitated from CKO intermediate thymocytes was more highly sulfenylated than that from wild-type intermediate thymocytes (Fig. 6e), which, given the highly unstable nature of protein sulfenic acids *in vivo*<sup>38</sup>, probably represented an underestimation. The enhanced sulfenylation of Bcl-2 in CKO thymocytes was not the result of a greater abundance of ROS, as wild-type thymocytes and CKO thymocytes showed similar abundance of cellular ROS (Supplementary Fig. 6k). Notably, as the ROS scavenger NAC prevented the degradation of Bcl-2 in and apoptosis of cultured intermediate CKO thymocytes (Fig. 6f,g), our findings suggested that thymocytes were instead more susceptible to degradative ROS-induced protein modification when deficient in CHMP5.

We hypothesized that because of the defect in Bcl-2 expression in CKO thymocytes, inhibition of apoptosis *in vivo* would restore thymocyte development in CKO mice. Indeed, we found that genetic ablation of Bim, a key mediator of thymocyte apoptosis<sup>39</sup>, as well as transgenic overexpression of Bcl-2, significantly augmented post-selection thymocyte development in CKO mice, as evinced by the restoration of TCR $\beta^+$ CCR7 $hi$  thymocytes and CD4 $^+$  or CD8 $^+$  single-positive thymocytes in these mice (Fig. 6h,i and Supplementary Fig. 7a–d). CKO mice on the Bim $^{-/-}$  genetic background had 3.6-fold more CD4SP thymocytes and 2.6-fold more CD8SP thymocytes

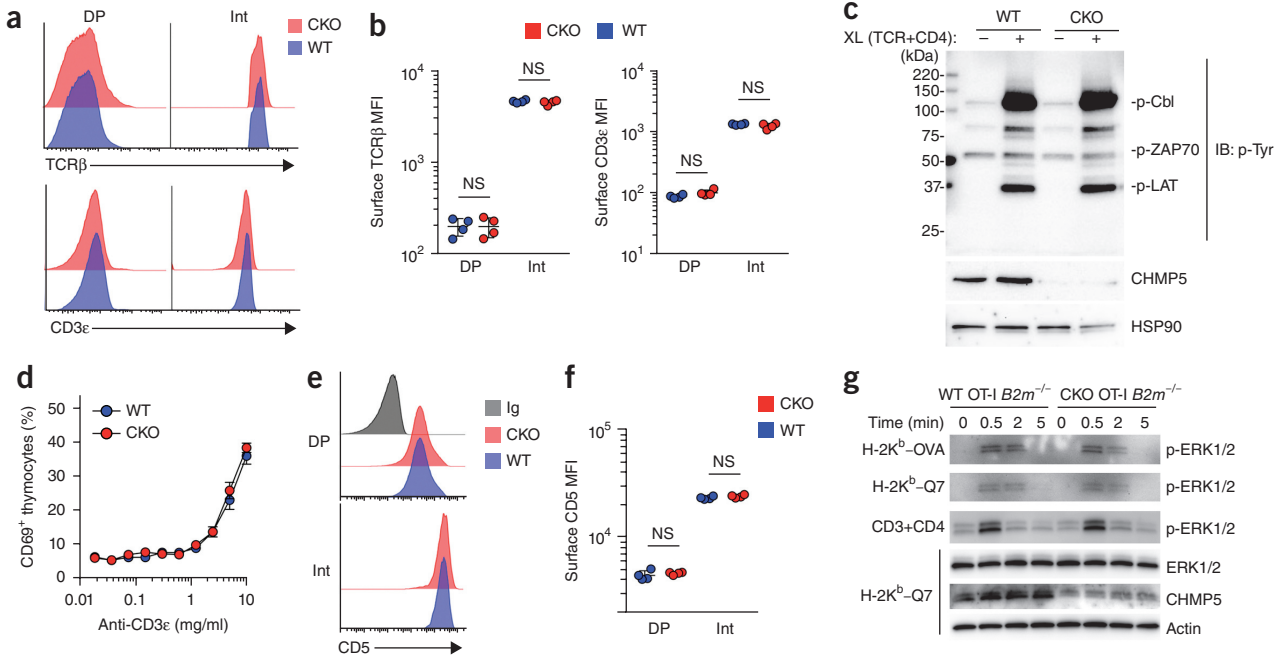


**Figure 4** Normal TCR signaling in CHMP5-deficient thymocytes. (a,b) Flow cytometry analyzing the surface expression of TCR $\beta$  and CD3 $\epsilon$  on wild-type and CKO thymocytes (a), and mean fluorescence intensity (MFI) of that expression (b). NS, 0.9881, 0.4606, 0.870 and 0.2902 (left to right) (Student's *t*-test). (c) Immunoblot analysis (IB) of various phosphorylated (p-) proteins (right margin), probed with antibody (4G10) to phosphorylated tyrosine (p-Tyr) (top), as well as total CHMP5 and HSP90 (loading control) (below), in whole-cell lysates of wild-type and CKO thymocytes (above blots) left unstimulated (-) stimulated (+) for 10 min via cross-linking (XL) with anti-TCR $\beta$  plus anti-CD4 (TCR+CD4) (above lanes). Left margin, molecular size (in kilodaltons (kDa)). (d) Frequency of CD69 $^{+}$  thymocytes among wild-type and CKO cells (key) stimulated overnight (18 h) with anti-CD3 $\epsilon$  ('titrated' concentrations; horizontal axis) plus anti-CD4 (fixed at 5  $\mu$ g/ml). (e,f) Flow cytometry analyzing the surface expression CD5 on wild-type and CKO (key) thymocyte subsets (left margin) (e), and mean fluorescence intensity of that expression (f). Ig (immunoglobulin), isotype-matched control antibody. NS, 0.4500 (left) and 0.1771 (right) (Student's *t*-test). (g) Immunoblot analysis of phosphorylated (p-) ERK1 and ERK2 (ERK1/2) in wild-type and CKO OT-I  $B2m^{-/-}$  thymocytes (above blots) stimulated (left margin) with the high-affinity (agonist) tetramer H-2K $b$ -OVA or the low-affinity (antagonist) tetramer H-2K $b$ -Q7, or by antibody cross-linking with anti-CD3 $\epsilon$  plus anti-CD4 (CD3+CD4; positive control) (top four blots), as well as total ERK, CHMP5 and HSP90 (loading control) in wild-type and CKO OT-I  $B2m^{-/-}$  thymocytes stimulated with H-2K $b$ -Q7 (below); all images of bands were obtained with the same exposure. Each symbol (b,f) represents an individual mouse ( $n = 4$  per group); small horizontal lines indicate the mean ( $\pm$  s.d.). Data are representative of five independent experiments (a,b,d-f; average  $\pm$  s.e.m. of  $n = 4$  mice per group in d) or two independent experiments (c,g).

than did CKO mice on the *Bim* $^{+/+}$  genetic background (Fig. 6h,i). We thus concluded that the apoptosis of CKO thymocytes was due at least in part to downregulation of Bcl-2 protein. Furthermore, these results supported our hypothesis that post-translational stabilization of Bcl-2 by CHMP5 enables the survival of post-selection thymocytes and, ultimately, the productive generation of T cells during positive selection.

#### TCR signals control CHMP5 expression in thymocytes

We next explored whether the abundance of CHMP5 was controlled during thymocyte selection. Even though the induction of CHMP5 expression in intermediate thymocytes that had received signaling via the TCR suggested that it was stabilized by positive selection, *in vitro* stimulation with anti-TCR plus crosslinking of the co-receptors CD2 or CD28, with ionomycin alone or with PMA plus ionomycin downregulated CHMP5 expression in DP thymocytes (Supplementary Fig. 8a). Suspecting that those agonists might have exceeded the physiological thresholds for TCR signaling during positive selection<sup>23</sup>, we quantified CHMP5 expression in DP thymocytes stimulated with 'titrated' doses of PMA plus ionomycin. Notably, we found that the expression of CHMP5 was increased only by low or intermediate doses of PMA plus ionomycin but was downregulated at higher doses (Fig. 7a).

The graded modulation of CHMP5 expression by the dose of PMA plus ionomycin suggested that CHMP5 in DP thymocytes

might sense the quantity of TCR signals. To test this possibility with more physiological TCR ligands, we measured CHMP5 in preselection OT-I  $B2m^{-/-}$  DP thymocytes stimulated with a panel of tetramers of H-2K $b$  and OVA-derived peptides<sup>23–25</sup>. Indeed, we found that CHMP5 was stabilized only by low-affinity (antagonist) tetramer ligands (Q7, G4 and E1), while high-affinity (agonist) ligands (OVA and A2), like the high dose of PMA plus ionomycin, downregulated its expression (Fig. 7b). In fact, both high concentrations of PMA plus ionomycin and agonist tetramers caused downregulation of the expression of *Chmp5* mRNA and CHMP5 protein (Supplementary Fig. 8b,c). As expected, we detected more apoptosis of OT-I  $B2m^{-/-}$  CKO preselection thymocytes stimulated with low-affinity tetramer than of their wild-type counterparts (Fig. 7c).

Because such analyses proved technically challenging in thymocytes, we used HEK293 cells and human Jurkat T lymphocytes to determine whether TCR signaling caused ubiquitination of CHMP5 that might have led to its degradation. We determined that in these cells, a high dose of PMA plus ionomycin or crosslinking with anti-CD3 plus anti-CD28 indeed induced ubiquitination of CHMP5 and Bcl-2 that was inhibited by NAC (Supplementary Fig. 8d–f). These results confirmed that the degradation of CHMP5 protein was induced by strong TCR agonists and was associated with ROS-dependent degradation of Bcl-2.

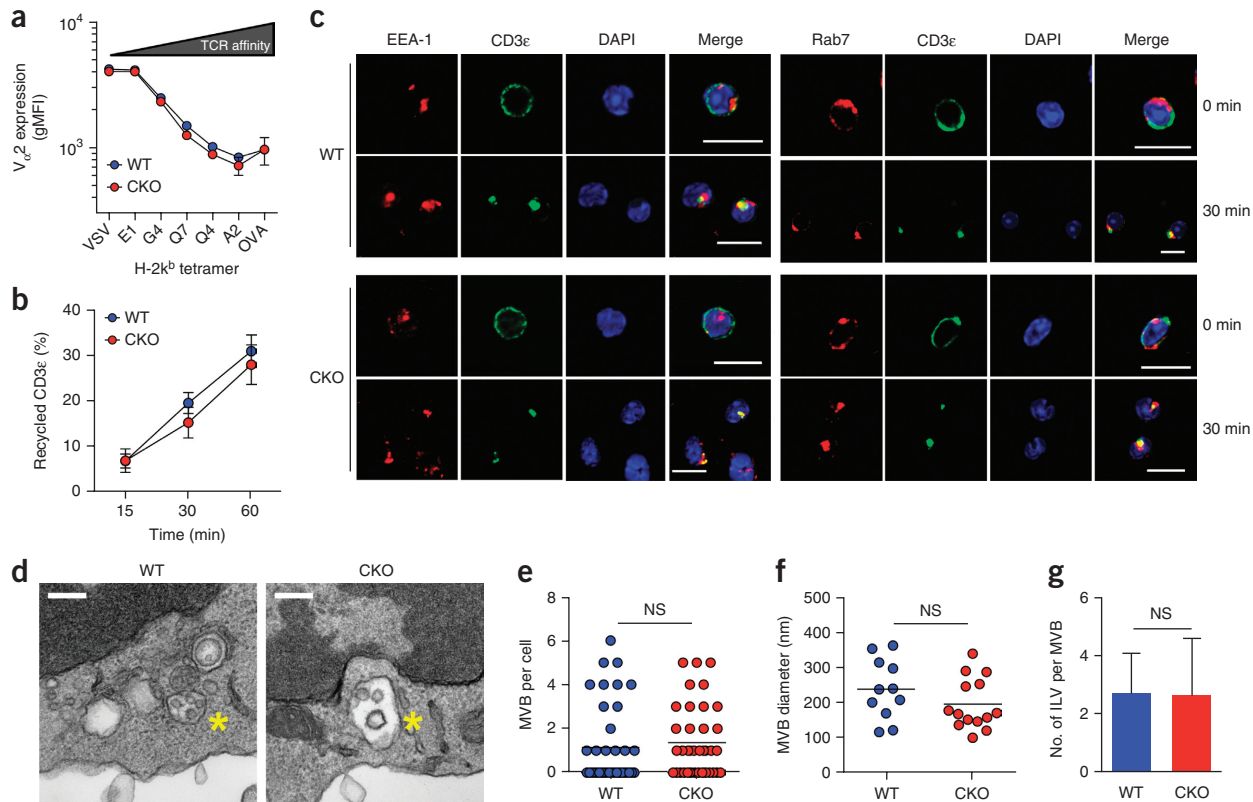


**Figure 5** Assessment of ESCRT-machinery activity in thymocytes. **(a)** Surface expression of V<sub>α</sub>2 (TCR) on wild-type and CKO OT-I *B2m*<sup>−/−</sup> thymocytes stimulated with H-2K<sup>b</sup> tetramers loaded with various peptides (horizontal axis) of ‘graded’ affinity for the TCR (low to high (left to right); wedge above plot), presented as geometric mean fluorescence intensity (gMFI). **(b)** Steady-state recycling of CD3ε in intermediate wild-type and CKO thymocytes. **(c)** Confocal microscopy of wild-type and CKO CD4<sup>+</sup>CD8<sup>+</sup> double-positive thymocytes left unstimulated (0) or stimulated for 30 min with anti-TCR (right margin), showing the internalization of CD3ε into early (EEA-1<sup>+</sup>) endosomes (left group) or late (Rab7<sup>+</sup>) endosomes (right group). DAPI, DNA-binding dye. Scale bars, 10 μm. **(d)** Transmission electron microscopy of MVBs (yellow asterisks) in wild-type and CKO intermediate thymocytes (above images). Scale bars, 200 nm. **(e–g)** Quantification of MVBs (**e**), MVB diameter (**f**) and quantification of intraluminal vesicles (ILV) per MVB (**g**) in wild-type and CKO intermediate thymocytes. Each symbol (**e,f**) represents an individual cell; small horizontal lines indicate the mean. NS, 0.586 (e), 0.1966 (f) and 0.9101 (g) (Student’s *t*-test). Data are representative of three independent experiments (average ± s.e.m. of *n* = 4 mice per group (**a,b**); error bars (**g**), s.d.).

### Post-translational modification of CHMP5

To elucidate the mechanism by which CHMP5 was regulated, we performed mass spectrometry to determine whether this was post-translational modification via TCR signaling. Specifically, we obtained affinity-purified Flag-tagged CHMP5 from lysates of HEK293 cells treated with a low dose of PMA plus ionomycin and subjected the CHMP5 to phosphoproteome mass spectrometry. Accordingly, we identified ligand-induced post-translational modifications of CHMP5, which included phosphorylation at Ser26 and Ser30 and ubiquitination at Lys100, residues that were strictly conserved across various mammalian species (Fig. 7d).

Through the use of site-directed mutagenesis and biochemical assays, we investigated the specific contribution of those residues to the stability of CHMP5. First, we determined (in pulse-chase assay) that replacement of the lysine at position 100 with arginine increased the stability of CHMP5 in HEK293 cells (Fig. 7e), probably by limiting the polyubiquitination of CHMP5 (Fig. 7f). That result indicated involvement of Lys100 in the agonist-induced degradation of CHMP5. Conversely, individual or combined substitution of the serine at position 26 with glycine (S26G) and substitution of the serine at position 30 with alanine (S30A), which nullify serine-phosphorylation, resulted in constitutive ubiquitination of CHMP5 (Fig. 7g); this suggested that phosphorylation of Ser26 and Ser30 was necessary for the stability of CHMP5.

### The deubiquitinase USP8 regulates CHMP5 stability

To achieve further mechanistic insight into the post-translational regulation of CHMP5, we considered that ligand-induced stabilization of CHMP5 might require specific deubiquitinases (DUBs). Thus, to screen for DUBs that regulated CHMP5, we co-transfected HEK293 cells to express epitope-tagged CHMP5 along with a panel of candidate DUBs and measured ubiquitination of CHMP5 after stimulating the cells with a high dose of PMA plus ionomycin. In this screen, we identified USP8 and USP21 as DUBs that inhibited the ubiquitination of CHMP5 (Fig. 8a). As USP21 is dispensable for T cell development<sup>40</sup>, while deletion of USP8 impairs T cell generation<sup>41</sup> similar such impairment in to CKO mice, we focused on USP8 as a potential CHMP5-specific deubiquitinase. Overexpression of USP8 potently inhibited the ubiquitination of CHMP5 (Fig. 8b) and increased the stability of CHMP5 in HEK293 cells (Fig. 8c).

Expression of USP8 protein was upregulated in thymocytes<sup>41</sup> independently of CHMP5 (Supplementary Fig. 9a), and USP8 immunoprecipitated together with CHMP5 in intermediate DP thymocytes but not in DP thymocytes that had not undergone TCR selection signaling (Fig. 8d and Supplementary Fig. 9b); this suggested that positive selection signals induced the interaction of USP8 with CHMP5. Correspondingly, we detected CHMP5-USP8 association in DP thymocytes stimulated with a low dose of PMA plus ionomycin

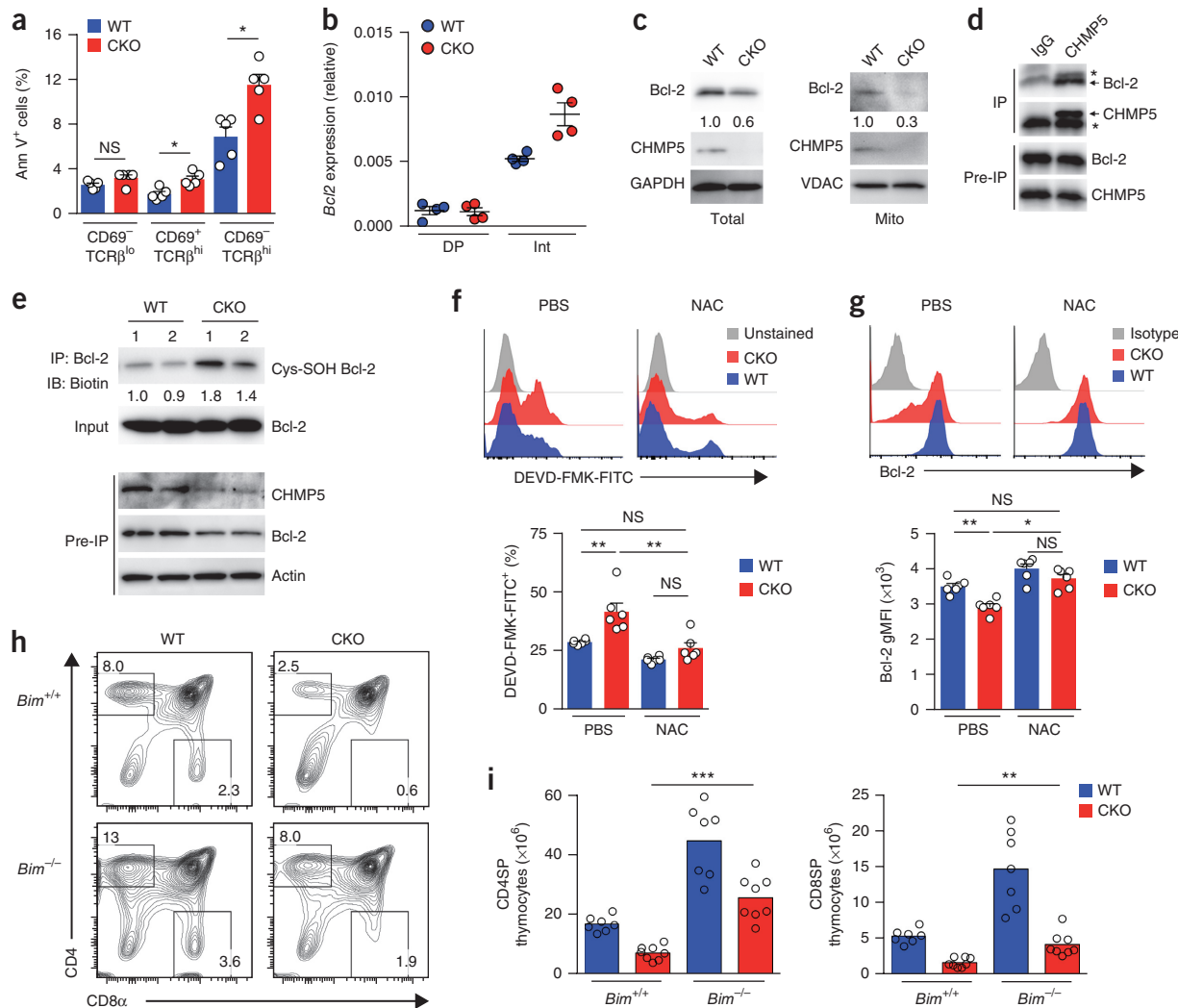


**Figure 6** Post-transcriptional stabilization of Bcl-2 by CHMP5 ensures the survival of post-selection in thymocytes. (a) Frequency of annexin V-positive (AnnV<sup>+</sup>) cells among various thymocyte subsets (below plot) from wild-type and CKO mice (key). (b) *Bcl2* mRNA expression in sorted wild-type and CKO (key) thymocyte subsets (blow plot); results are presented relative to those of mRNA from the control gene *Actb*. (c) Immunoblot analysis of Bcl-2 and CHMP5 in total lysates (left) and mitochondrial fractions (Mito) of wild-type and CKO intermediate thymocytes (above lanes); numbers below lanes indicate Bcl-2 band intensity relative to that of wild-type cells. (d) Immunoblot analysis of Bcl-2 and CHMP5 in lysates of wild-type intermediate thymocytes before (Pre-IP) and after (IP) immunoprecipitation with anti-CHMP5 or isotype-matched control antibody (IgG) (above lanes); asterisks (right margin) indicate antibody light chain. (e) Immunoblot analysis of sulfenylated (Cys-OH) Bcl-2 in lysates of wild-type and CKO intermediate thymocytes (two mice (1, 2) above lanes) per genotype) before (Input; second blot) and after (top blot) immunoprecipitation with anti-Bcl-2 (equal amounts in each lane); numbers below lanes indicate band intensity relative to that of wild-type samples. Below, immunoblot analysis of Bcl-2, CHMP5 and β-actin (loading control throughout) in lysates of cells as above, before immunoprecipitation. (f,g) Flow cytometry (top) analyzing DEVD-FMK-FITC fluorescence (f) and intracellular Bcl-2 (g) in wild-type and CKO thymocytes (key) treated with PBS or NAC (above plots); below, quantification of results above. Unstained, unstained cells; Isotype, isotype-matched control antibody. (h,i) Flow cytometry of cells from CKO mice ( $n = 8$ ) or their wild-type littermates ( $n = 7$ ) (above plots) on the *Bim*<sup>+/+</sup> ( $n = 7$  mice) or *Bim*<sup>-/-</sup> ( $n = 8$  mice) genetic background (left margin) (h), and absolute number of CD4<sup>+</sup> or CD8<sup>+</sup> single-positive thymocytes in those mice (i). Numbers adjacent to outlined areas (h) indicate percent CD4<sup>+</sup>CD8α<sup>+</sup> cells (top left) or CD4<sup>+</sup>CD8α<sup>+</sup> cells (bottom right). Each symbol (a,f,g,i) represents an individual mouse. \* $P < 0.05$ , \*\* $P < 0.001$  and \*\*\* $P < 0.0001$  (Student's *t*-test). Data are representative of three (a–c) or two (d–g) independent experiments (error bars, s.e.m. of  $n = 5$  mice per group (a) or six mice per group (f,g)) or are pooled from three experiments (h,i).

(which stabilized CHMP5) but not in those stimulated with a high dose of PMA plus ionomycin (Supplementary Fig. 9c). Furthermore, cell-free assays indicated direct physical interaction of CHMP5 with USP8 (Fig. 8e).

Because the S26G and S30A substitutions resulted in constitutive degradation of CHMP5, we considered that Ser26 and Ser30 might control the interaction of CHMP5 with USP8, which specifically inhibited the ubiquitination of CHMP5 and improved its stability (Fig. 8a–c). Co-immunoprecipitation of epitope-tagged proteins

revealed interaction between USP8 and wild-type CHMP5 but not between USP8 and mutant CHMP5 with both substitutions (S26G and S30A) (Fig. 8f). Thus, we surmised that phosphorylation at residues Ser26 and Ser30 promoted the stability of CHMP5 at least in part by facilitating its interaction with USP8.

Finally, to assess the *in vivo* role of USP8 in the stability of CHMP5, we quantified CHMP5 expression in lysates of USP8-deficient intermediate thymocytes (from *Usp8*<sup>fl/fl</sup> mice expressing the *Cd4*-Cre transgene (*Usp8*<sup>CD4cre</sup>))<sup>41</sup>. Notably, loss of USP8 resulted in a decrease not

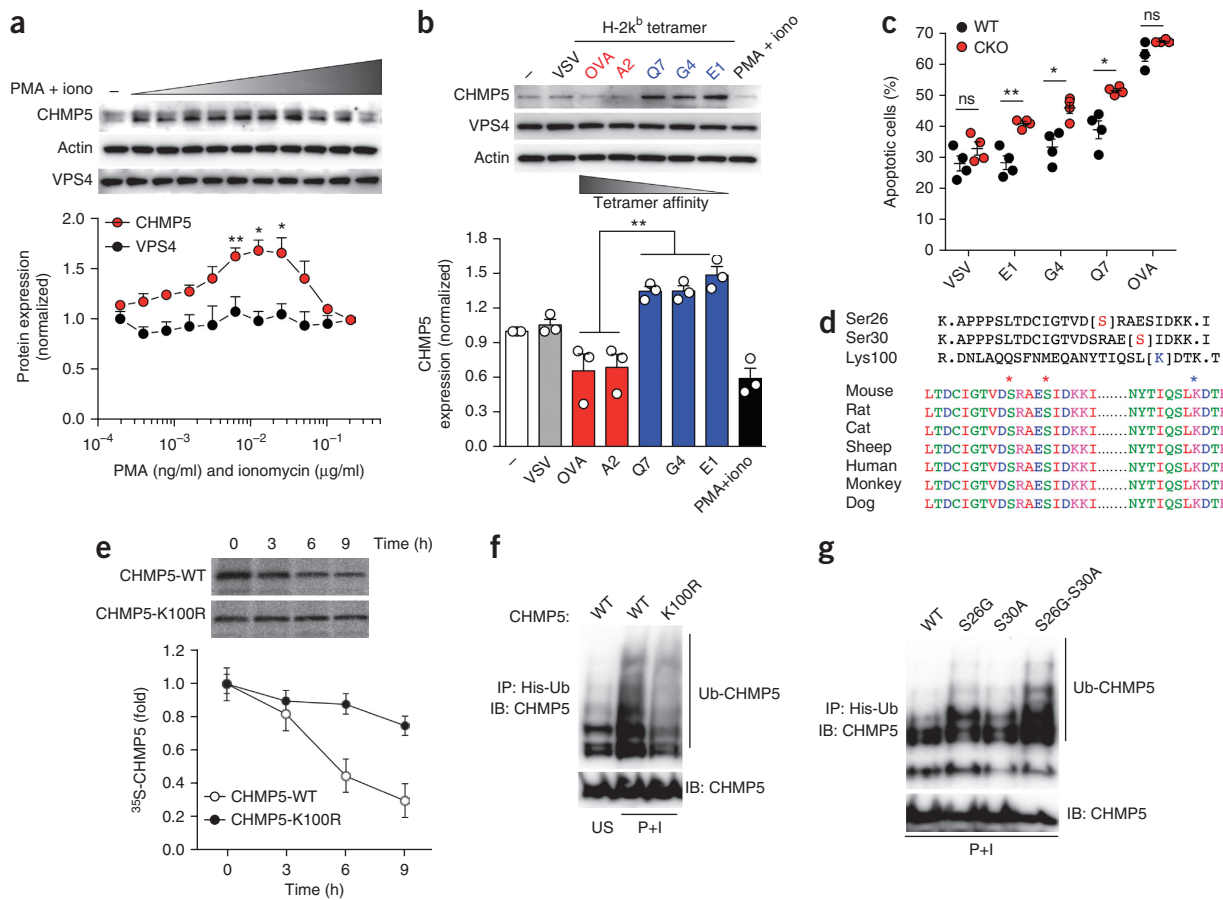


**Figure 7** Post-translational regulation of CHMP5 expression by TCR signaling. **(a,b)** Immunoblot analysis (top) of CHMP5 and VPS4 in OT-I  $B2m^{-/-}$  preselection CD4 $^{+}$ CD8 $^{+}$  double-positive thymocytes left unstimulated (–) or stimulated with ‘titrated’ concentrations (wedge) of PMA and ionomycin (a) or with various tetramers of H-2K $^{b}$  (above lanes) or PMA and ionomycin (far right) (b); below, quantification of the expression of CHMP5 or VPS4 (key) (a) or CHMP5 (b) in the cells above, presented as band intensity, normalized to that of  $\beta$ -actin and unstimulated cells. \* $P < 0.05$  and \*\* $P < 0.001$ , compared with unstimulated cells in a, and bracketed comparison in b (Student’s *t*-test (a) or one-way analysis of variance with Tukey’s post-hoc test (b)). **(c)** Frequency of apoptotic cells among OT-I  $B2m^{-/-}$  thymocytes obtained from wild-type and CKO mice (key) and stimulated with various tetramers of H-2K $^{b}$  (horizontal axis). \* $P < 0.05$  and \*\* $P < 0.001$  (Student’s *t*-test). **(d)** CHMP5 residues modified in Jurkat T cells stimulated with PMA plus ionomycin, as detected by mass spectrometry (top: left margin and red or blue font in parentheses, modified residues), and alignment of the CHMP5 protein sequences of selected mammalian species (bottom: amino acids distinguished by color; asterisks indicate residues modified). **(e)** Immunoblot analysis of <sup>35</sup>S-labeled wild-type CHMP5 (CHMP5-WT) and mutant CHMP5 with replacement of the lysine at position 100 with arginine (CHMP5-K100R) in HEK293 cells at 0–9 h during a pulse-chase analysis (top), and quantification of the abundance of <sup>35</sup>S-labeled CHMP5 in those cells over time, relative to that at time 0, set as 1. **(f,g)** Immunoblot analysis (IB) of ubiquitinated (Ub-) CHMP5 (top) or total CHMP5 (bottom) in HEK293 cells transfected to express epitope-tagged wild-type or mutant CHMP5 as in e (f) or with the S26G or S30A substitution or both (S26G-S30A) (g) (above lanes) and left unstimulated (US) or stimulated with PMA plus ionomycin (below blot), assessed with (top) or without (bottom) immunoprecipitation of histidine-tagged ubiquitin (IP: His-Ub). Each symbol (b,c) represents an individual mouse; small horizontal lines (c) indicate the mean ( $\pm$  s.e.m.). Data are from four (a) or three (b) independent experiments (average  $\pm$  s.e.m.) or are representative of two experiments with four mice per group (c) or two independent experiments (e–g).

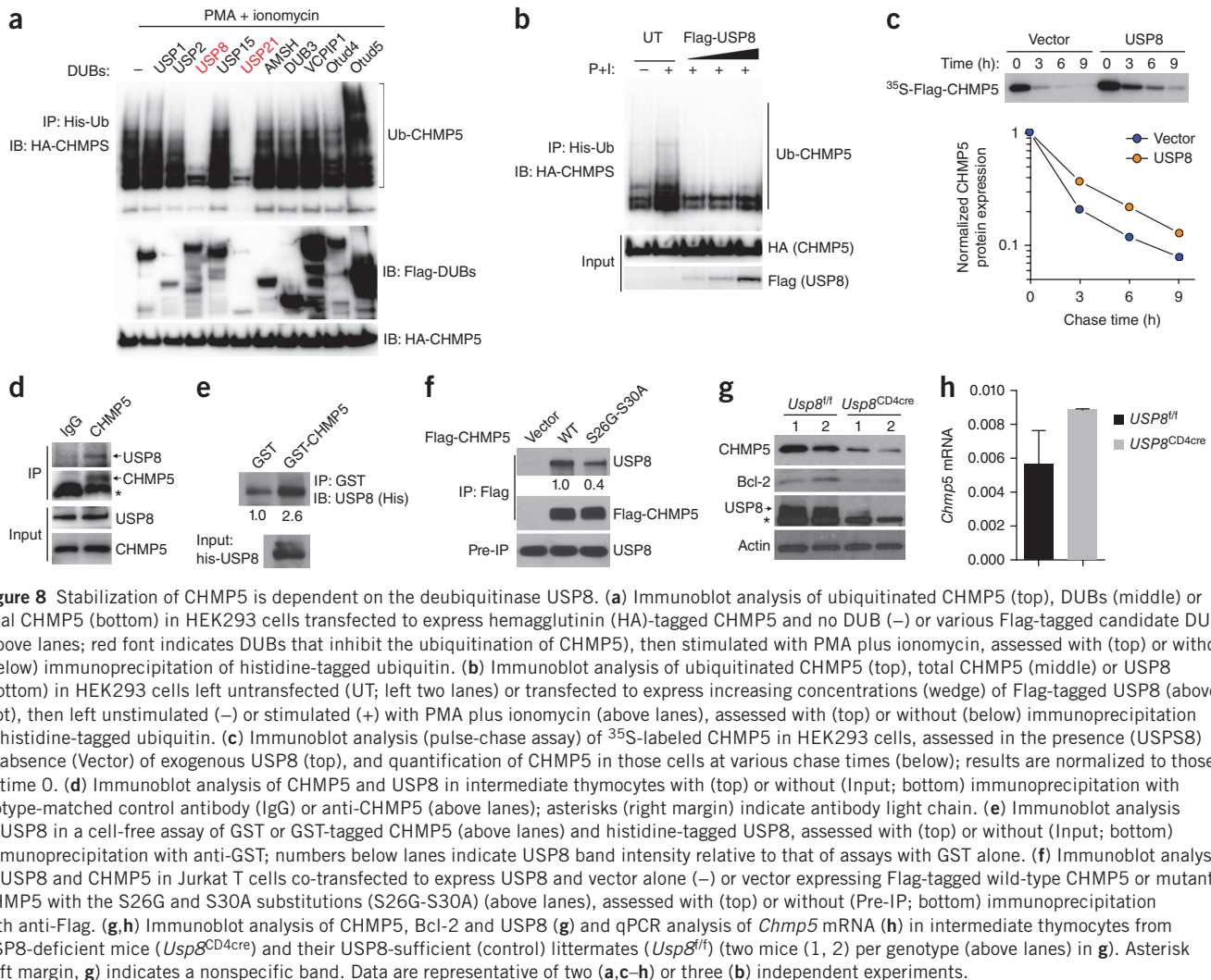
only in CHMP5 but also in Bcl-2 (Fig. 8g). The loss of CHMP5 and Bcl-2 was at the protein level, as the expression of both *Chmp5* mRNA and *Bcl2* mRNA was intact in these cells (Fig. 8h and Supplementary Fig. 9d). Together our results have identified CHMP5 as an integral component of the post-translational machinery that enables the positive selection of thymocytes and have identified a USP8–CHMP5 complex that controls the survival of post-selection thymocytes downstream of TCR signaling (Supplementary Fig. 9e).

## DISCUSSION

In this study, we reported the finding that the ESCRT protein CHMP5 is an essential factor that enables T cell development in a cell-autonomous manner. Specifically, independently of its role in the ESCRT machinery, CHMP5 orchestrated post-translational events necessary for

the survival of thymocytes undergoing positive selection. In the absence of CHMP5, thymocytes failed to complete positive selection and T cell development was abolished. Our results suggest that the induction of CHMP5, which peaked at the intermediate thymocyte development stage, represents a previously undefined and critical checkpoint of positive selection. CHMP5 itself was also specifically regulated by post-translational mechanisms that were intricately regulated by TCR signaling. Collectively, these findings demonstrate that beyond their classical function in membrane remodeling, individual ESCRT proteins have non-canonical activities that are critical for tissue development.

The abundance of CHMP5 was regulated differentially by TCR signal affinity. Through the use of TCR-specific tetramers with pre-defined affinities, we determined that low-affinity TCR ligands that



induce positive selection uniquely promoted CHMP5 expression by increasing the stability of CHMP5, not via the transcription of *Chmp5*. CHMP5 in turn ensured the stability of Bcl-2 in positively selected thymocytes, which enabled their survival and maturation into the peripheral T cell pool. Thus, stabilization of CHMP5 appears to be one mechanism by which positive-selection TCR signals are able to induce and adequately sustain Bcl-2 to ensure the survival of differentiating thymocytes. Notably, in contrast, high-affinity ligands that induce negative selection by apoptosis downregulated the expression of both CHMP5 protein and *Chmp5* mRNA, an outcome replicated in CKO mice, with the consequence being the abolition of T cell maturation. It is conceivable that *in vivo* downregulation of *Chmp5* mRNA by high-affinity ligands, combined with downregulation of CHMP5 protein, would serve to guarantee the effective and timely elimination of potentially self-reactive thymocytes during selection. Further studies are needed to determine whether this differential modulation of CHMP5 stability represents a discriminatory mechanism that broadly ‘translates’ the quantity of both high-affinity TCR signaling and low-affinity TCR signaling to central tolerance<sup>1</sup>.

ROS-induced oxidation can regulate protein activity positively or negatively<sup>38</sup>. In particular, ROS-mediated cysteine sulfenylation induced the degradation of Bcl-2, which suggested that CHMP5 might protect Bcl-2 from deleterious oxidation by ROS. Thus, it is

perhaps not coincidental that the activity of CHMP5 ‘mapped’ to intermediate thymocytes, in which several ROS are generated by TCR signaling during positive selection<sup>42,43</sup>. Moreover, intermediate thymocytes represent the earliest post-selection developmental stage at which Bcl-2 proteins are first induced by intrathymic signaling either via the TCR or via IL-7 (refs. 2,22). Nevertheless, while our results support the proposal that Bcl-2 is a true target of CHMP5 involved in the phenotype of CKO mice, the partial restoration of the development of CHMP5-deficient thymocytes by genetic ablation of *Bim* or by transgenic overexpression of Bcl-2 suggests the existence of additional CHMP5 substrates involved in regulating positive selection. Future identification of these substrates should yield additional insight into the activity of CHMP5.

CHMP5-deficient thymocytes unexpectedly showed no major defects in MVB biogenesis, endocytosis, surface-receptor recycling or degradation or TCR signaling despite the involvement of the ESCRT machinery and CHMP5 in these processes<sup>7,10,11,44</sup>. The normal TCR dynamics in CHMP5-deficient thymocytes also contrasted with increased surface TCR expression and signaling in Jurkat T cells in which CHMP5 is knocked down<sup>45</sup>. Such discrepancies might reflect a difference in the function of CHMP5 in thymocytes relative to that in peripheral or mature T cells or in primary T cells relative to that in transformed T cell lines. Alternatively, it might indicate redundancy

in activators of VPS4, as has been suggested, in which in the absence of CHMP5, the ESCRT machinery achieves activation of VPS4 via VPS2 (also known as CHMP2 and Did4)<sup>31,32</sup>, which is also expressed in thymocytes. In any case, our results suggest that the role of CHMP5 in positive selection is probably independent of its function in ESCRT-mediated endocytosis.

Paradoxically, even though the ESCRT machinery evolved to facilitate the lysosomal degradation of ubiquitin-tagged proteins<sup>46</sup>, our findings for thymocytes suggested an activity of CHMP5 that instead promoted the stability of protein substrates such as Bcl-2. One possible explanation for this is that CHMP5 deficiency might have restored or augmented the activity of an undefined Bcl-2-specific E3 ligase whose lysosomal degradation was reversed in the absence of CHMP5-dependent ESCRT machinery. However, as we did not observe major defects in ESCRT-mediated processes, we favor a scenario in which CHMP5 directly impairs the ubiquitination of specific protein targets. That possibility is supported by the finding of direct physical association between CHMP5 and Bcl-2 in post-selection thymocytes. Indeed, interactions between members of the ESCRT complex and proteins of the Bcl-2 family have been reported in yeast, in which an isoform of the ESCRT-III protein VPS24 binds to the Bcl-2-associated protein Bax and inhibits its pro-apoptotic activity<sup>47</sup>.

We identified USP8 as a specific deubiquitinase for CHMP5, which indicates the involvement of a CHMP5-USP8 complex in controlling the positive selection of thymocytes. In agreement with that, expression of CHMP5 protein was substantially downregulated in USP8-deficient thymocytes, and the observed T cell deficiency in mice with thymocyte-specific USP8 deficiency<sup>41</sup> resembles the phenotype of the CKO mice reported here. Despite the lack of specific structural domains in CHMP5, crystallography studies suggest that the C-terminal tandem β-hairpin structure of CHMP5, which binds the ESCRT accessory protein Brox, furnishes a protein–protein interaction interface<sup>48</sup> that could potentially be involved in binding USP8. Our identification of serine phosphorylation residues in CHMP5 that facilitated its binding to USP8 not only emphasize the specificity and signal dependence of this association but evoke similarities to the serine phosphorylation required for the interaction of USP8 with the adaptor 14-3-3β that is also essential for T-cell development<sup>41</sup>.

In summary, our study has identified the ESCRT protein CHMP5 as a critical requirement for the positive selection of thymocytes and T cell development. Evidence that CHMP5 is also anti-apoptotic in acute myeloid leukemia cells<sup>49</sup> raises the possibility that its dysregulation might perturb tissue homeostasis and the emergence of malignancy. This highlights the need for future work to elucidate the link between CHMP5 and disease.

## METHODS

Methods, including statements of data availability and any associated accession codes and references, are available in the [online version of the paper](#).

*Note:* Any Supplementary Information and Source Data files are available in the [online version of the paper](#).

## ACKNOWLEDGMENTS

We thank A. Singer (US National Institutes of Health) for *Bcl2*-transgenic mice; S. Dimmeler (J.W. Goethe University, Frankfurt, Germany) for *Bcl-2*-encoding plasmids; J. Kaplan (University of Utah) for anti-LIP5; M. Greenblatt for critical reading of the manuscript; J. McCormick (Weill Cornell Medicine) for sorting by flow cytometry; L. Cohen-Gould, J. Cohen and J. Jimenez for histology and electron microscopy; and the NIH Tetramer Core Facility (Emory University) for tetramers. Supported by the US National Institutes of Health (R01AR068983 to J.H.S., and R01CA112663 to L.H.G.).

## AUTHOR CONTRIBUTIONS

S.A. designed study, performed experiments, analyzed data and wrote the manuscript; K.H.P., S.E.B., R.L. and H.R.S. assisted with experiments; H.S. and J.H.K. performed bioinformatics; K.-PK. provided mice with *loxP*-flanked *Usp8* alleles; J.-H.S. designed the study, performed experiments, analyzed data and wrote the manuscript; and L.H.G. designed the study, analyzed data, provided supervision and wrote the manuscript.

## COMPETING FINANCIAL INTERESTS

The authors declare competing financial interests: details are available in the [online version of the paper](#).

Reprints and permissions information is available online at <http://www.nature.com/reprints/index.html>. Publisher's note: Springer Nature remains neutral with regard to jurisdictional claims in published maps and institutional affiliations.

1. Starr, T.K., Jameson, S.C. & Hogquist, K.A. Positive and negative selection of T cells. *Annu. Rev. Immunol.* **21**, 139–176 (2003).
2. Singer, A., Adoro, S. & Park, J.H. Lineage fate and intense debate: myths, models and mechanisms of CD4- versus CD8-lineage choice. *Nat. Rev. Immunol.* **8**, 788–801 (2008).
3. Bonifacino, J.S. *et al.* Novel post-translational regulation of TCR expression in CD4+CD8+ thymocytes influenced by CD4. *Nature* **344**, 247–251 (1990).
4. Grimm, L.M., Goldberg, A.L., Poirier, G.G., Schwartz, L.M. & Osborne, B.A. Proteasomes play an essential role in thymocyte apoptosis. *EMBO J.* **15**, 3835–3844 (1996).
5. Yang, Y., Fang, S., Jensen, J.P., Weissman, A.M. & Ashwell, J.D. Ubiquitin protein ligase activity of IAPs and their degradation in proteasomes in response to apoptotic stimuli. *Science* **288**, 874–877 (2000).
6. Maseda, D., Meister, S., Neubert, K., Herrmann, M. & Voll, R.E. Proteasome inhibition drastically but reversibly impairs murine lymphocyte development. *Cell Death Differ.* **15**, 600–612 (2008).
7. Rusten, T.E., Vaccari, T. & Stennmark, H. Shaping development with ESCRTs. *Nat. Cell Biol.* **14**, 38–45 (2011).
8. Merrill, S.A. & Hanson, P.I. Activation of human VPS4A by ESCRT-III proteins reveals ability of substrates to relieve enzyme autoinhibition. *J. Biol. Chem.* **285**, 35428–35438 (2010).
9. Shim, S., Merrill, S.A. & Hanson, P.I. Novel interactions of ESCRT-III with LIP5 and VPS4 and their implications for ESCRT-III disassembly. *Mol. Biol. Cell* **19**, 2661–2672 (2008).
10. Kranz, A., Kinner, A. & Kölling, R. A family of small coiled-coil-forming proteins functioning at the late endosome in yeast. *Mol. Biol. Cell* **12**, 711–723 (2001).
11. Shim, J.H. *et al.* CHMP5 is essential for late endosome function and down-regulation of receptor signaling during mouse embryogenesis. *J. Cell Biol.* **172**, 1045–1056 (2006).
12. Greenblatt, M.B. *et al.* CHMP5 controls bone turnover rates by dampening NF-κB activity in osteoclasts. *J. Exp. Med.* **212**, 1283–1301 (2015).
13. Chang, Y.C. *et al.* mdm2 and bax, downstream mediators of the p53 response, are degraded by the ubiquitin-proteasome pathway. *Cell Growth Differ.* **9**, 79–84 (1998).
14. Nencioni, A. *et al.* Evidence for a protective role of Mcl-1 in proteasome inhibitor-induced apoptosis. *Blood* **105**, 3255–3262 (2005).
15. van Ewijk, W., Shores, E.W. & Singer, A. Crosstalk in the mouse thymus. *Immunol. Today* **15**, 214–217 (1994).
16. Bendelac, A., Matzinger, P., Seder, R.A., Paul, W.E. & Schwartz, R.H. Activation events during thymic selection. *J. Exp. Med.* **175**, 731–742 (1992).
17. Yamashita, I., Nagata, T., Tada, T. & Nakayama, T. CD69 cell surface expression identifies developing thymocytes which audition for T cell antigen receptor-mediated positive selection. *Int. Immunol.* **5**, 1139–1150 (1993).
18. Barnden, M.J., Allison, J., Heath, W.R. & Carbone, F.R. Defective TCR expression in transgenic mice constructed using cDNA-based α- and β-chain genes under the control of heterologous regulatory elements. *Immunol. Cell Biol.* **76**, 34–40 (1998).
19. Matusek, T. *et al.* The ESCRT machinery regulates the secretion and long-range activity of Hedgehog. *Nature* **516**, 99–103 (2014).
20. Azzam, H.S. *et al.* CD5 expression is developmentally regulated by T cell receptor (TCR) signals and TCR avidity. *J. Exp. Med.* **188**, 2301–2311 (1998).
21. Ueno, T. *et al.* CCR7 signals are essential for cortex-medulla migration of developing thymocytes. *J. Exp. Med.* **200**, 493–505 (2004).
22. Yu, Q. *et al.* Cytokine signal transduction is suppressed in preselection double-positive thymocytes and restored by positive selection. *J. Exp. Med.* **203**, 165–175 (2006).
23. Fu, G. *et al.* Themis sets the signal threshold for positive and negative selection in T-cell development. *Nature* **504**, 441–445 (2013).
24. Hogquist, K.A. *et al.* T cell receptor antagonist peptides induce positive selection. *Cell* **76**, 17–27 (1994).
25. Daniels, M.A. *et al.* Thymic selection threshold defined by compartmentalization of Ras/MAPK signalling. *Nature* **444**, 724–729 (2006).
26. Mingueneau, M. *et al.* The transcriptional landscape of αβ T cell differentiation. *Nat. Immunol.* **14**, 619–632 (2013).
27. Carpenter, A.C. & Bosselut, R. Decision checkpoints in the thymus. *Nat. Immunol.* **11**, 666–673 (2010).

28. Gerondakis, S., Fulford, T.S., Messina, N.L. & Grumont, R.J. NF- $\kappa$ B control of T cell development. *Nat. Immunol.* **15**, 15–25 (2014).
29. Xing, Y., Wang, X., Jameson, S.C. & Hogquist, K.A. Late stages of T cell maturation in the thymus involve NF- $\kappa$ B and tonic type I interferon signaling. *Nat. Immunol.* **17**, 565–573 (2016).
30. Hurley, J.H. & Emr, S.D. The ESCRT complexes: structure and mechanism of a membrane-trafficking network. *Annu. Rev. Biophys. Biomol. Struct.* **35**, 277–298 (2006).
31. Azmi, I.F. *et al.* ESCRT-III family members stimulate Vps4 ATPase activity directly or via Vta1. *Dev. Cell* **14**, 50–61 (2008).
32. Rue, S.M., Mattei, S., Sakseña, S. & Emr, S.D. Novel Ist1-Did2 complex functions at a late step in multivesicular body sorting. *Mol. Biol. Cell* **19**, 475–484 (2008).
33. Gallo, E.M. *et al.* Calcineurin sets the bandwidth for discrimination of signals during thymocyte development. *Nature* **450**, 731–735 (2007).
34. Staton, T.L. *et al.* Dampening of death pathways by schnurri-2 is essential for T-cell development. *Nature* **472**, 105–109 (2011).
35. Czabotar, P.E., Lessene, G., Strasser, A. & Adams, J.M. Control of apoptosis by the BCL-2 protein family: implications for physiology and therapy. *Nat. Rev. Mol. Cell Biol.* **15**, 49–63 (2014).
36. Azad, N. *et al.* Role of oxidative/nitrosative stress-mediated Bcl-2 regulation in apoptosis and malignant transformation. *Ann. NY Acad. Sci.* **1203**, 1–6 (2010).
37. Luanpitpong, S. *et al.* Regulation of apoptosis by Bcl-2 cysteine oxidation in human lung epithelial cells. *Mol. Biol. Cell* **24**, 858–869 (2013).
38. Holmström, K.M. & Finkel, T. Cellular mechanisms and physiological consequences of redox-dependent signalling. *Nat. Rev. Mol. Cell Biol.* **15**, 411–421 (2014).
39. Bouillet, P. *et al.* BH3-only Bcl-2 family member Bim is required for apoptosis of autoreactive thymocytes. *Nature* **415**, 922–926 (2002).
40. Pannu, J. *et al.* Ubiquitin specific protease 21 is dispensable for normal development, hematopoiesis and lymphocyte differentiation. *PLoS One* **10**, e0117304 (2015).
41. Dufner, A. *et al.* The ubiquitin-specific protease USP8 is critical for the development and homeostasis of T cells. *Nat. Immunol.* **16**, 950–960 (2015).
42. Devadas, S., Zaritskaya, L., Rhee, S.G., Oberley, L. & Williams, M.S. Discrete generation of superoxide and hydrogen peroxide by T cell receptor stimulation: selective regulation of mitogen-activated protein kinase activation and fas ligand expression. *J. Exp. Med.* **195**, 59–70 (2002).
43. Jin, R. *et al.* Trx1/TrxR1 system regulates post-selected DP thymocytes survival by modulating ASK1-JNK/p38 MAPK activities. *Immunol. Cell Biol.* **93**, 744–752 (2015).
44. Choudhuri, K. *et al.* Polarized release of T-cell-receptor-enriched microvesicles at the immunological synapse. *Nature* **507**, 118–123 (2014).
45. Wi, S.M., Min, Y. & Lee, K.Y. Charged MVb protein 5 is involved in T-cell receptor signaling. *Exp. Mol. Med.* **48**, e206 (2016).
46. Raiborg, C. & Stenmark, H. The ESCRT machinery in endosomal sorting of ubiquitylated membrane proteins. *Nature* **458**, 445–452 (2009).
47. Khouri, C.M., Yang, Z., Ismail, S. & Greenwood, M.T. Characterization of a novel alternatively spliced human transcript encoding an N-terminally truncated Vps24 protein that suppresses the effects of Bax in an ESCRT independent manner in yeast. *Gene* **391**, 233–241 (2007).
48. Mu, R. *et al.* Two distinct binding modes define the interaction of Brox with the C-terminal tails of CHMP5 and CHMP4B. *Structure* **20**, 887–898 (2012).
49. Shahmoradgoli, M. *et al.* Antiapoptotic function of charged multivesicular body protein 5: a potentially relevant gene in acute myeloid leukemia. *Int. J. Cancer* **128**, 2865–2871 (2011).

## ONLINE METHODS

**Mice.** C57BL/6J mice, B6.SJL-*Ptprc<sup>a</sup>Pepc<sup>b</sup>*/BoyJ (B6.SJL) mice, C57BL/6-Tg(TcrαTcrβ)425Cbn/J (OT-II) mice, C57BL/6-Tg(TcrαTcrβ)1100Mjb/J (OT-I) mice, B6.129P2-B2m<sup>tm1Unc</sup>/J ( $\beta_2$ -microglobulin-deficient) mice, B6.129S2-H2dlAb1-Ea/J (MHC class II-deficient) mice, B6.129S1-Bcl2l11tm1.1Ast/J (*Bim*<sup>-/-</sup>) mice<sup>39</sup> and B6.Cg-Tg(Cd4-cre)1Cwi/BfluJ (*Cd4*-Cre-transgenic) mice<sup>50</sup> were purchased from the Jackson Laboratory. OT-I *B2m*<sup>-/-</sup> mice were bred in our colony at Weill Cornell Medical College (New York). *Chmp5*<sup>fl/fl</sup> mice (with *loxP*-flanked exons 4 and 5 of *Chmp5*) have been previously described<sup>11</sup>. *Bcl2*-transgenic mice<sup>51</sup> were provided by A. Singer (NIH). All mice were maintained in a specific-pathogen-free facility at Weill Cornell Medical College (New York) under approved protocols and were analyzed between 6 weeks and 12 weeks of age.

**Cell isolation, culture and stimulation.** Thymus, spleen and lymph nodes were harvested and processed by mechanical dissociation to obtain single cells. Splenocytes were treated with ACK buffer (Gibco) to lyse red cells. Single-cell suspensions were filtered through 70-μm strainers and were resuspended in T cell media (RPMI 1640 supplemented with 2 mM L-glutamine, 1 mM sodium pyruvate, 10 mM HEPES, pH 7.4, 1× MEM nonessential amino acids, 50 IU/ml penicillin, 50 μg/ml streptomycin, 55 μM  $\beta$ -mercaptoethanol and 10% FBS). HEK293 cells (ATCC) were cultured in complete DMEM supplemented with 10% FBS, 2 mM L-glutamine, 50 IU/ml penicillin and 50 μg/ml streptomycin. Except where indicated otherwise, thymocytes were stimulated with pre-determined doses of plate-bound antibody or pharmacological agonists<sup>52,53</sup>: 10 μg/ml anti-TCR (H57-597, BD Biosciences), 5 μg/ml anti-mouse CD2 (RM2-5, BD Biosciences), 5 μg/ml anti-mouse CD4 (GK1.5, BD Biosciences); 0.2 ng/ml PMA (phorbol-myristate-acetate) plus 0.2 μg/ml ionomycin (Calbiochem); 50 μg/ml cycloheximide (Sigma); 10 μM MG132 (Sigma); and 5 ng/ml IL-7 (PeproTech). All cells were cultured at 37 °C in 5% CO<sub>2</sub> incubators.

**Antibodies, flow cytometry and cell sorting.** Single-cell suspensions were washed with flow-cytometry buffer (PBS plus 2% FBS) and were stained with fluorochrome-conjugated antibodies for 45 min at 4 °C. The following antibody clones were used: anti-CD4 (GK1.5), anti-CD8 $\alpha$  (53-6.7), anti-TCR $\beta$  (H57-597), anti-CD3 $\epsilon$  (145-2C11), anti-CD24 (M1/69), anti-CD69 (H1.2F3), anti-CD44 (IM7), anti-CCR7 (4B12), anti-CD5 (53-7.3), anti-V $\alpha$ 2 (B20.1), anti-IL-7R $\alpha$  (A7R34) and anti-CD45.1 (A20), anti-CD45.2 (104), all from BioLegend; and anti-V $\beta$ 5 (MR9-4) and anti-Bcl-2 (clone 3F11), both from BD Biosciences. For intracellular protein detection, cells were first stained for surface antigen, then were fixed, permeabilized and stained for intracellular proteins following the Foxp3 staining kit protocol (eBiosciences). STAT5 phosphorylated at Tyr694 (clone 47/Stat5(pY694); BD Biosciences) was detected using the BD Phosflow protocol. Samples were acquired on a BD LSRII. Dead cells were excluded by DAPI (4',6-diamidino-2-phenylindole, 0.5 μg/ml; Life Technologies) or, for fixed cells, positivity for Live/Dead fixable Yellow (Life Technologies). All flow-cytometry sorting was performed on a BD FACSAria II SORP instrument. Sorted thymocyte populations were defined as follows: preselection CD4 $^+$ CD8 $\alpha$  $^+$  double-positive (DP), CD4 $^+$ CD8 $\alpha$  $^+$ CD24 $^{hi}$ CD69 $^-$ TCR $\beta$  $^{neg-lo}$ ; intermediate (Int; **Supplementary Fig. 4a**), CD4 $^+$ CD8 $\alpha$  $^{int}$ CD24 $hi$ CD69 $^+$ TCR $\beta$  $^{hi}$ ; and post-selection, CD24 $^-$ CD69 $^-$ TCR $\beta$  $^{hi}$ . Flow-cytometry data were analyzed using FlowJo vX.0.7 (TreeStar).

**Tetramer stimulation.** H-2k $b$  tetramer peptides were generated by the NIH Tetramer Core Facility (Emory University): VSV (RGYVYQGL), OVA (SIINFEKL), A2 (SAINFEKL), Q7 (SIINFEQL), G4 (SIIGFEKL) and E1 (EIINFEKL). OT-I *B2m*<sup>-/-</sup> or *Chmp5*<sup>fl/fl</sup>CD4-Cre OT-I *B2m*<sup>-/-</sup> thymocytes were stimulated with tetramers as previously described<sup>23,54</sup>. In brief, for apoptosis assays and determination of the surface expression of V $\alpha$ 2, 0.5 × 10<sup>6</sup> thymocytes were plated in 200 μl T cell medium in 96-well U-bottomed plates and were stimulated by the addition of 2 μl tetramer (final, 0.2 μg/ml) and were cultured for 4 h. For immunoblot analysis, 2 × 10<sup>6</sup> thymocytes were stained with tetramer (0.2 μg/ml tetramer per 0.5 × 10<sup>6</sup> cells) on ice in Eppendorf tubes. Cells were activated by warming up to 37 °C with pre-warmed (37 °C) PBS and incubation in 37 °C water bath for the times indicated in **Figure 4g**. Tetramer-stimulated thymocytes were analyzed by flow cytometry or were subjected to immunoblot analysis.

**Receptor internalization and recycling assay.** For receptor internalization, tetramer-stimulated OT-I *B2m*<sup>-/-</sup> or *Chmp5*<sup>fl/fl</sup>CD4-Cre OT-I *B2m*<sup>-/-</sup> thymocytes (as described above) were evaluated for surface V $\alpha$ 2 geometric mean fluorescence intensity in FlowJo. The CD3 $\epsilon$ -recycling assay was performed with some modifications of previously described protocols<sup>55,56</sup>. In brief, 20 × 10<sup>6</sup> total thymocytes were cultured in medium containing 5 μg/ml phycoerythrin (PE)-labeled anti-CD3 $\epsilon$  (145-2C11, BD Biosciences) for 30 min and were washed twice in PBS. Thymocytes were then acid-stripped (30 s at 25 °C in 100 mM glycine and 100 mM NaCl, pH 2.5) to remove surface-bound antibodies and washed twice in PBS, and aliquots were incubated at 37 °C, for the times indicated in **Figure 5b**, to allow receptor recycling to the surface. At the end of each time, thymocytes were mixed with ice-cold PBS containing 1% BSA and 0.1% NaN<sub>3</sub> and were maintained on ice. After data for all time points were collected, thymocytes were washed and acid-stripped (100 mM glycine and 100 mM NaCl, pH 2.5), followed by washing in ice-cold PBS (containing 1% BSA and 0.1% NaN<sub>3</sub>). Thymocytes were stained for CD4, CD8 $\alpha$ , CD69, CD24 and TCR $\beta$  (antibodies identified above) and were analyzed by flow cytometry. CD3 $\epsilon$  recycling was calculated by the following formula: % recycled = 100 × [(MFI at t = 0) – (MFI at time point)]/(MFI at t = 0)].

**Bone-marrow transplantation.** Bone marrow (BM) was isolated by flushing of tibia and femur marrows with ACK red cell lysis buffer (Gibco), then it was washed and depleted of B cells and T-cells using CD19 microbeads and a CD3 $\epsilon$  microbeads kit (Miltenyi Biotec). For 1:1 mixed chimeras, BM obtained from wild-type (*Chmp5*<sup>fl/fl</sup>, CD45.2 $^+$ ) or CKO (*Chmp5*<sup>fl/fl</sup>CD4-Cre; CD45.2 $^+$ ) mice and depleted of T cells and B cells (1 × 10<sup>6</sup> BM cells) was mixed with BM obtained from congenic wild-type (B6.SJL, CD45.1 $^+$ ) mice and depleted of T cells and B cells (1 × 10<sup>6</sup> BM cells) and the mixture was injected into lethally irradiated (1,000 rads) congenic wild-type (B6.SJL, CD45.1 $^+$ ) mice. For lentiviral transduction, BM was depleted of T cells and B cells and the resultant BM cells were cultured in complete StemPro-34 SFM (ThermoFisher Scientific) containing recombinant mouse cytokines (10 ng/ml IL-3, 50 ng/ml IL-6, 20 ng/ml Flt3L and 50 ng/ml SCF, PeproTech), 50 IU/ml penicillin and 50 μg/ml streptomycin. After 24 h, cells were infected with lentiviral supernatants in the presence of Polybrene (8 μg/ml) and centrifugation at 1,000g for 2 h at 25 °C. Total transduced cells were harvested after 48 h and was injected by the retro-orbital route into lethally irradiated congenic wild-type (B6.SJL, CD45.1 $^+$ ) mice. All chimeras were analyzed at 8–12 weeks after transplantation.

**Immunofluorescence microscopy.** Thymocytes were stained with 5 μg/ml anti-CD3 $\epsilon$  (145-2C11, hamster; BD Biosciences) on ice for 30 min and were transferred onto pre-chilled poly-L-lysine-coated glass slides (Sigma) that were previously coated with anti-mouse CD3 $\epsilon$  (17A2, 5 μg/ml; eBiosciences). Cells were allowed to attach to slides on wet ice for 30 min. For stimulation, slides were placed in 37 °C incubator for the times indicated in **Figure 4c**, after which they were fixed for 10 min at 25 °C with 4% paraformaldehyde. After being fixed, cells were washed five times with PBS, were blocked and permeabilized by incubation for 30–60 min in PBS containing 3% goat serum, 1% BSA and 0.1% Triton X-100. Slides were then incubated overnight at 4 °C with primary antibodies (rabbit anti-EEA1 (C45B10; 1:200) and rabbit anti-Rab7 (D95F2; 1:200; Cell Signaling Technology) in PBS containing 1% BSA and 0.1% Triton X-100. Primary antibodies were visualized by staining with secondary antibodies (Alexa Fluor 488-conjugated goat anti-hamster (A21110; Life Technologies) and VectaFluor R.T.U. Dylight 594 anti-rabbit IgG (DI-1794; Vector Laboratories)) and were counterstained with 1 μg/ml DAPI. Stained sections were mounted with Slowfade Gold (Life Technologies) and were imaged using an AxioVert LSM710 confocal microscope (Zeiss).

**Histology.** Harvested thymus were snap-frozen in O.C.T. compound (Tissue-Tek, Sakura) and were stored at -80 °C. 10-μm sections were cut at -18 °C using a Bright OTF5000 cryostat (Hacker Instruments) and were stained with hematoxylin and eosin.

**Transmission electron microscopy (TEM).** Sorted thymocytes were washed once in PBS and were either directly fixed for TEM as described below or incubated with 10 μg/ml anti-CD3 $\epsilon$  biotin (145-2C11, BD Biosciences) in serum-free (SF) RPMI on ice for 30 min. Stained cells were washed in PBS and

incubated for 1 h at 37 °C in SF-RPMI containing 15 µg/ml of 10-nm gold-conjugated streptavidin (AC-10-04-05; Cytodiagnostic) and 15 µg/ml of 5-nm gold-conjugated human holo-transferrin (AC-5-07-05; Cytodiagnostic). After culture, cells were washed twice with PBS before TEM fixing. In brief, cells were fixed for TEM with a modified Karnovsky's fix of 2.5% glutaraldehyde, 4% paraformaldehyde and 0.02% picric acid in 0.1 M sodium cacodylate buffer at pH 7.2. Following secondary fixation in 1% osmium tetroxide and 1.5% potassium ferricyanide, samples were dehydrated through a graded ethanol series and were embedded in an epon analog resin. Ultrathin sections were cut using a Diatome diamond knife (Diatome) on an RMC MT-7000 Ultramicrotome (RMC Products). Sections were collected on copper grids and were further contrasted with lead citrate and viewed on a JEM 1400 electron microscope (JEOL) operated at 120 kV. Images were recorded with a Veleta 2K × 2K CCD (Olympus-SIS) and images were evaluated and quantified by researchers 'blinded' to sample identity.

**RNA isolation and quantitative real-time PCR.** Total RNA was isolated from cells using Qiazol reagent (Qiagen). Total RNA (100–500 ng) was reverse-transcribed to cDNA using a high-capacity cDNA reverse-transcription kit with random priming (Applied Biosystems, #4368814). Gene-expression levels were calculated and are presented as expression relative to that of control genes (*Actb* or *Hprt*) on the basis of the change in cycling threshold ( $\Delta C_T$ ) method as  $2^{-\Delta C_T}$ , where  $\Delta C_T$  is  $C_T$  (gene of interest) –  $C_T$  (control gene). PCR primer sequences and TaqMan probes are in **Supplementary Table 1**.

**Plasmids and lentiviruses.** The following plasmids were used: Flag- or HA-tagged human USP1, USP2, USP8, USP15, USP21, AMSH, DUB3, VCP1P1, OTUD4 and OTUD5 (Addgene); Myc-tagged human USP8 (Sino Biological Inc.); shRNA targeting human CHMP5 and USP8 (Sigma). Plasmids encoding Bcl-2 were provided by N. Du (Weill Cornell Medicine) and S. Dimmeler (J.W. Goethe University Hospital)<sup>57</sup>. *Chmp5* cDNA encoding C-terminal Flag-tagged CHMP5 (NP\_084090.1) or N-terminal HA-tagged CHMP5 was amplified by PCR and cloned into pCDNA3 (ThermoScientific), pCI-Neo (Promega), or pHAGE/IRES-GFP. CHMP5 mutants (S26G, S30A, S26G-S30A and K100R) were generated by site-directed mutagenesis of a wild-type *Chmp5* construct (Agilent Technologies). *BCL2* encoding N-terminal HA-tagged Bcl-2 (NP\_000624.2) was amplified by PCR and cloned into the pCMV-Myc (Clontech) mammalian expression vector. To produce lentivirus, 293-FT cells (Invitrogen) were transfected with plasmids along with VSVg and delta 8.9 packaging plasmid vectors. After 48 h, viral supernatants were harvested, filtered through a 0.45-µm filter and concentrated with an Amicon Ultra-10 centrifugal filter (EMD Millipore).

**Immunoprecipitation, immunoblot analysis and pulse-chase assay.** Thymocytes were washed in ice-cold PBS and centrifuged and pellets were stored at –80 °C or lysed immediately in TNT buffer (10 mM Tris, pH 8.0, 50 mM NaCl, 5 mM EDTA, 2 mM NaF, 30 mM sodium pyrophosphate, 100 mM Na<sub>3</sub>VO<sub>4</sub>, 0.5 mM PMSF, 1 µg/ml leupeptin, 5 µg/ml aprotinin and 1% Triton X-100). Mitochondrial fractions were prepared using the Mitochondrial Isolation kit (ThermoFisher Scientific). Lysates were subjected to immunoprecipitation or were separated by SDS-PAGE before transfer to Immunobilon-P membranes for detection. For pulse-chase assays, HEK293 cells were transfected with DNA constructs using Effectene reagent (QIAGEN). After 48 h, transfected cells were incubated under starvation conditions (3% FBS Cys/Met-free DMEM) for 3 h. Cells were then incubated in labeling medium containing <sup>35</sup>S-methionine for 1 h and were cultured in chase medium (5% FBS in complete DMEM) for various durations. Cells were lysed, and proteins were immunoprecipitated with anti-Flag (M2)-conjugated agarose and subjected to SDS-PAGE and immunoblot analysis. The following antibodies were used: anti-CHMP5 (Santa Cruz, sc-67230; 1:250 for immunoprecipitation (IP) and 1:1,000 for IB), polyclonal antibody to CHMP5 generated in-house by immunization of rabbits with a 17-amino-acid synthetic peptide corresponding to the C-terminal sequence of mouse CHMP5<sup>12</sup> (antibody specificity validation, **Supplementary Fig. 1a**; 1:100 for immunoprecipitation (IP) and 1:1,000 for IB), anti-Bcl-2 (sc-7382; 1:250 for IB), anti-Bim (sc-11425; 1:250 for IB), anti-ubiquitin (sc-8017; 1:250 for IB), anti-Vps4 (sc-393428; 1:250 for IB), anti-Hsp90 (sc-7947; 1:250 for IB), anti-Gata-3 (sc-268; 1:250 for IB), anti-

HA agarose conjugate (sc-7392AC, clone F7; 1:40 for IP), anti-c-Myc HRP-conjugate (sc-40AC, clone 9E10; 1:1,000 for IB) and anti-HA HRP conjugate (sc-7392; 1:1,000 for IB), all from Santa Cruz; anti-ERK (4695; 1:1,000 for IB), antibody to ERK1/2 phosphorylated at Thr202 and Tyr204 (4576; 1:1,000 for IB), VDAC (4866; 1:1,000 for IB), anti-actin (4967; 1:1,000 for IB), anti-Hrs (15087; 1:1,000 for IB) and anti-Bcl-xL (2764; 1:1000 for IB), all from Cell Signaling Technologies; antibody to phosphorylated tyrosine (clone 4G10, 05-321; 1:1,000 for IB), from EMD Millipore; anti-Mcl-1 (Rockland, 600-401-394; 1:1,000 for IB); anti-GAPDH (Affinity Bioreagents, PA-116777; 1:1,000 for IB); anti-USP8 (Genetex, GTX103747; 1:1,000 for IB); anti-CHMP2B (Abcam, ab157208; 1:1,000 for IB); anti-LIP5/VTA1 (a gift J. Kaplan, University of Utah; 1:1,000 for IB); and anti-Flag (Sigma-Aldrich, F-1804; 1:1,000 for IB). Labeled proteins were visualized with autoradiography or by digital chemiluminescence imaging (FluorChem E, ProteinSimple) and densitometry quantification was performed using the ImageJ program (NIH).

**Ubiquitination assay.** HEK293 cells were transfected with plasmids encoding human CHMP5, USP8 and Bcl-2, along with plasmid encoding histidine (His)-tagged ubiquitin. 24 h after transfection, the cells were treated with 10 µM MG132 (EMD Millipore) for 6 h and harvested for biochemical assays. In some cases, HEK293 cells were also treated with 0.2 ng/ml PMA plus 0.2 µg/ml ionomycin. To detect ubiquitination cells were harvested, lysed and sonicated in denaturation buffer (8M Urea, 50 mM Tris, pH 8.0, 1.0% Triton X-100 and 10 mM Imidazol), immunoprecipitated with Ni-NTA beads and analyzed by immunoblot with antibodies (identified above) specific for the target proteins.

**Cysteine-sulfenic-acid detection.** Bcl-2 oxidation was assessed by cysteine-sulfenic-acid detection using the DCP-Bio1 reagent (3-(2,4-dioxocyclohexyl) propyl) as described<sup>37,58</sup>. In brief, thymocytes were labeled with the cysteine oxidation probe DCP-Bio1 (EMD Millipore, NS-1226) in lysis buffer (50 mM Tris-HCl, pH 7.5, 100 mM NaCl, 0.1% SDS, 0.5% sodium deoxycholate, 0.5% NP-40, 0.5% Triton X-100, 50 mM NaF, 1 mM PMSF, 1 mM DCP-Bio1, 100 µM DTPA, 10 mM N-ethylmaleimide, 10 mM iodoacetamide, 200 U/ml catalase and 1× protease inhibitor cocktail) for 2 h on ice. The DCP-Bio1-labeled proteins were immunoprecipitated with anti-Bcl-2 (identified above) and protein A-conjugated Dynabeads. Lysates were separated by SDS-PAGE, transferred to Immunomobilon-P membranes and developed with streptavidin-conjugated anti-HRP (SA10001, 1:3000; Life Technologies).

**ROS and apoptosis detection.** Cellular ROS were measured by incubation of equal numbers of thymocytes from wild-type and CKO mice in serum-free medium containing 5 µM CellRox Deep Red reagent (Life Technologies), followed by incubation for 30 min at 37 °C and then flow cytometry. NAC (N-acetyl-L-cysteine) was dissolved in PBS and adjusted to a pH of 7.4, and was used in cultures at a final concentration of 1 mM. Apoptotic cells were detected by annexin-V staining or by detection of active caspase-3 using the DEVD-FMK-FITC CaspGLOW reagent (eBiosciences).

**NF-κB activity.** 10 µg of sorted thymocyte cell lysates prepared with RIPA extraction buffer (ThermoFisher Scientific) were assayed in duplicates for active NF-κB subunit p65 with a commercially available p65 ELISA kit and protocol (ADI-EKS-446, Enzo Life Sciences) and with TNF-stimulated HeLa cell nuclear extract as a positive control. The chemiluminescent substrate signals were determined with a Varioskan (Thermo Electron Corporation), and data are presented as relative light units.

**Mass spectrometry.** For phosphorylation and ubiquitination-site mapping of CHMP5, HEK293 cells were transfected to express Flag-tagged mouse CHMP5 and, after 24 h, were treated with PMA and ionomycin and 10 µM MG132. 6 h later, cells were lysed and CHMP5 proteins were immunoprecipitated with anti-Flag conjugated to agarose (M2 beads, Sigma) and were eluted by Flag peptides. CHMP5 eluates were subjected to SDS-PAGE and visualized by colloidal Coomassie blue. The CHMP5 band was excised and was treated with DTT to reduce disulfide bonds and iodoacetamide to derivatize cysteine residues. The protein was digested in-gel with trypsin and then was analyzed by nanoscale-microcapillary reversed-phase liquid chromatography-tandem

mass spectrometry as described previously<sup>59</sup>. Tandem mass spectrometry spectra were searched using the SEQUEST algorithm<sup>60</sup> against a database containing the sequences of mouse CHMP5 and common contaminants such as mouse keratin proteins with static modification of cysteine carboxymethylation, dynamic modification of methionine oxidation, and phosphorylation of serine, threonine and tyrosine. All peptide matches were filtered on the basis of mass deviation, tryptic state and XCorr and were confirmed by manual validation.

**Statistics.** Sample sizes were chosen on the basis of previous experience with similar studies; no statistical tests were used to predetermine sample size, and no exclusion of data points was used. The number of times experiments were repeated is indicated in each figure legend. Except where indicated otherwise, comparison of differences between groups was determined with a two-tailed, unpaired Student's *t*-test and differences were considered significant at *P*<0.05. Statistical analysis was performed using GraphPad Prism 7.0.

**Data availability statement.** All supplementary information is available in the online version of the paper. Additional source data are available from the corresponding authors upon request.

50. Lee, P.P. *et al.* A critical role for Dnmt1 and DNA methylation in T cell development, function, and survival. *Immunity* **15**, 763–774 (2001).

51. Sentman, C.L., Shutter, J.R., Hockenberry, D., Kanagawa, O. & Korsmeyer, S.J. bcl-2 inhibits multiple forms of apoptosis but not negative selection in thymocytes. *Cell* **67**, 879–888 (1991).
52. Cibotti, R., Punt, J.A., Dash, K.S., Sharow, S.O. & Singer, A. Surface molecules that drive T cell development in vitro in the absence of thymic epithelium and in the absence of lineage-specific signals. *Immunity* **6**, 245–255 (1997).
53. Ohoka, Y. *et al.* In vitro differentiation and commitment of CD4+ CD8+ thymocytes to the CD4 lineage, without TCR engagement. *Int. Immunol.* **8**, 297–306 (1996).
54. Rybakin, V. & Gascoigne, N.R. Negative selection assay based on stimulation of T cell receptor transgenic thymocytes with peptide-MHC tetramers. *PLoS One* **7**, e43191 (2012).
55. Finetti, F. *et al.* Specific recycling receptors are targeted to the immune synapse by the intraflagellar transport system. *J. Cell Sci.* **127**, 1924–1937 (2014).
56. Myers, M.D., Dragone, L.L. & Weiss, A. Src-like adaptor protein down-regulates T cell receptor (TCR)-CD3 expression by targeting TCR $\zeta$  for degradation. *J. Cell Biol.* **170**, 285–294 (2005).
57. Breitschopf, K., Haendeler, J., Malchow, P., Zeiher, A.M. & Dimmeler, S. Posttranslational modification of Bcl-2 facilitates its proteasome-dependent degradation: molecular characterization of the involved signaling pathway. *Mol. Cell. Biol.* **20**, 1886–1896 (2000).
58. Nelson, K.J. *et al.* Use of dimedone-based chemical probes for sulfenic acid detection methods to visualize and identify labeled proteins. *Methods Enzymol.* **473**, 95–115 (2010).
59. Villén, J. & Gygi, S.P. The SCX/IMAC enrichment approach for global phosphorylation analysis by mass spectrometry. *Nat. Protoc.* **3**, 1630–1638 (2008).
60. Eng, J.K., McCormack, A.L. & Yates, J.R. An approach to correlate tandem mass spectral data of peptides with amino acid sequences in a protein database. *J. Am. Soc. Mass Spectrom.* **5**, 976–989 (1994).